Hierarchical architecture of dopaminergic circuits enables second-order conditioning in *Drosophila*

Daichi Yamada[1], Daniel Bushey[2], Li Feng[2], Karen Hibbard[2], Megan Sammons[2], Jan Funke[2], Ashok Litwin-Kumar[3], Toshihide Hige[1,4,5]*, Yoshinori Aso[2]*

1: Department of Biology, University of North Carolina at Chapel Hill, Chapel Hill, United States

2: Janelia Research Campus, Howard Hughes Medical Institute, Ashburn, United States

3: Department of Neuroscience, Columbia University, New York, United States

4: Department of Cell Biology and Physiology, University of North Carolina at Chapel Hill, Chapel Hill, United States

5: Integrative Program for Biological and Genome Sciences, University of North Carolina at Chapel Hill, Chapel Hill, United States

* Contact Info

hige@email.unc.edu

asoy@janelia.hhmi.org

Abstract

Dopaminergic neurons with distinct projection patterns and physiological properties compose memory subsystems in a brain. However, it is poorly understood whether or how they interact during complex learning. Here, we identify a feedforward circuit formed between dopamine subsystems and show that it is essential for second-order conditioning, an ethologically important form of higher-order associative learning. The *Drosophila* mushroom body comprises a series of dopaminergic compartments, each of which exhibits distinct memory dynamics. We find that a slow and stable memory compartment can serve as an effective “teacher” by instructing other faster and transient memory compartments via a single key interneuron, which we identify by connectome analysis and neurotransmitter prediction. This excitatory interneuron acquires enhanced response to reward-predicting odor after first-order conditioning and, upon activation, evokes dopamine release in the “student” compartments. These hierarchical connections between dopamine subsystems explain distinct properties of first- and second-order memory long known by behavioral psychologists.

Introduction

Knowledge about order and regularities in environments is crucial for animal survival. Although direct temporal correlation between stimuli and rewards is a primary drive for associative learning, animals are also capable of learning indirect relations between stimuli and rewards in many real-life situations. For example, bumble bees, who have prior foraging experience with other bees, can learn to visit a flower of a particular color without tasting nectar just by watching other bees sitting on flowers of that color (Avarguès-Weber and Chittka, 2014; Worden and Papaj, 2005a). In the case of humans, some TV commercials can be considered as conditioning of consumers to associate items with the positive valence that has been already associated with popular cartoon

characters. In both cases, learning depends on the valence of stimuli (i.e. sight of other bees or cartoon characters) that is acquired through prior experience. Although such higher-order associative learning is widely observed across species and ethologically important, its circuit mechanisms are poorly understood compared to those of simpler forms of associative learning.

Second-order conditioning is a major form of higher-order associative learning. In this learning paradigm, an initially neutral stimulus is paired with reward or punishment; that stimulus, which is now predictive of reward/punishment, then serves as an effective reinforcer when learning about a new stimulus. Since Pavlov's classic experiment with dogs (Pavlov, 1927), second-order conditioning has been demonstrated in various vertebrate and invertebrate models (Bitterman et al., 1983; Brembs and Heisenberg, 2001; Hawkins et al., 1998; Holland and Rescorla, 1975; Mizunami et al., 2009; Rizley and Rescorla, 1972; Sisk, 1976; Tabone and de Belle, 2011; Takeda, 1961). Furthermore, second-order conditioning is thought to extend the applicability of Pavlovian conditioning as an account of behaviors including observational learning (Avarguès-Weber and Chittka, 2014; Worden and Papaj, 2005b). Additionally, second-order conditioning has also served as a historically important tool for behavioral psychologists to study associative learning by giving them ample options to use virtually any stimulus as a reinforcer (Rescorla, 1980).

One prominent feature that characterizes second-order memory is its transiency, as originally noted by Pavlov and confirmed by other studies using various animal models (Herendeen and Chris Anderson, 1968; Stout et al., 2004; Yin et al., 1994). That is, the effectiveness of second-order conditioning usually reaches an asymptote after a small number of trials and begins to decline with further training (Gewirtz and Davis, 2000; Pavlov, 1927). This decline may be related to the fact that reward is constantly omitted during second-order conditioning. Another important feature of second-order

conditioning recognized by behavioral psychologists is that it does not form a tight association between the stimulus and the specific response elicited by the reinforcer, which is typically observed in first-order conditioning (Gewirtz and Davis, 2000; Pavlov, 1927). In other words, second-order learning seems to be based on general valence, rather than specific features, of reinforcers. These differences between first- and second-order memories raise important mechanistic questions: What is the circuit origin of those different memory features? Are they different because those two memories are stored in separate circuits that support distinct types of memories? If so, how do the two circuits interact when one memory instructs the other? Answering these questions requires precise mapping of second-order memory circuits.

In rodents, basolateral amygdala and dopaminergic neurons (DANs) play critical roles in second-order learning (Gewirtz and Davis, 1997; Maes et al., 2020). After first-order association, DANs in the ventral tegmental area acquire enhanced responses at the onset of the cue that predicts upcoming reward after conditioning (Schultz, 1998). A recent study used optogenetic silencing to demonstrate that such cue-evoked dopamine transients are essential for second-order conditioning (Maes et al., 2020). Whereas DANs consist of functionally diverse populations of neurons, each of which contributing to distinct types of learning (Roeper, 2013; Watabe-Uchida and Uchida, 2018), how these different DAN subtypes interact during second-order conditioning is completely unstudied.

The *Drosophila* mushroom body (MB), a dopamine-rich center for associative learning in insect brains, provides a tractable system to study the interaction between heterogeneous dopamine subsystems. *Drosophila* can perform second-order learning using olfactory or visual cues with punishment (Brembs and Heisenberg, 2001; Tabone and de Belle, 2011), although the underlying circuit mechanisms have not been examined. Decades of studies have revealed the anatomical and functional architecture

of the MB circuit (Figure 1A). Along the parallel axonal fibers of Kenyon cells (KCs), DANs and MB output neurons (MBONs) form 16 matched compartments (Aso et al., 2014; Li et al., 2020; Tanaka et al., 2008), which serve as units of associative learning. Reward and punishment activate distinct subsets of 20 types of DANs (Berry et al., 2015; Burke et al., 2012; Kirkhart and Scott, 2015; Lewis et al., 2015; Lin et al., 2014; Liu et al., 2012; Riemensperger et al., 2005; Siju et al., 2020). Individual DANs write and update memories in each compartment with cell-type-specific dynamics by modulating synaptic connection between KCs and MBONs (Aso et al., 2019, 2012; Aso and Rubin, 2016; Hige et al., 2015; Huetteroth et al., 2015; Owald et al., 2015; Perisse et al., 2016; Vrontou et al., 2021; Yamagata et al., 2015). Outside the MB, MBON axons project to regions where DAN dendrites arborize; this provides an anatomical pathway for feedback of memory-based information onto DANs, a potential substrate for higher-order conditioning. Indeed, early studies showed that DANs in the MB dynamically change odor responses after olfactory conditioning (Riemensperger et al., 2005). Furthermore, the recently completed EM connectome (Scheffer et al., 2020) revealed the full wiring diagram of the MB, including intricate connections from MBONs to the DANs. In both larval and adult *Drosophila*, large fractions of synaptic inputs to the MB's DANs originate from the MB itself (Eschbach et al., 2020; Li et al., 2020). Thus it is plausible that induction of synaptic plasticity in one compartment, in turn, affects how a learned stimulus activates DANs and becomes a secondary reinforcer. However, understanding the flow of information across compartments that underlies second-order conditioning is a challenging task, given that thousands of neurons are connected with DANs and MBONs.

Here, by exploiting connectomic data, we identify a key circuit that underlies second-order conditioning. We first establish a protocol for robust olfactory second-order conditioning with sugar reward. In contrast to stable odor-sugar first-order memory,

second-order memory decayed within a day and was highly susceptible to extinction. We next show that memory in α1, the compartment responsible for long-lasting appetitive memory (Ichinose et al., 2015; Yamagata et al., 2015), is most potent to promote second-order memory. The second-order memory instructed by α1 was transient during the training phase and extinction trials. Subsequent EM connectome and functional analysis identify a prominent cholinergic interneuron SMP108 that 1) forms an excitatory pathway from MBON-α1 to DANs in other compartments, 2) acquires an enhanced response to the reward-predicting odor, 3) can promote release of dopamine in multiple compartments, 4) is required for second-order conditioning, and 5) induces memory with fast and transient dynamics. Our study reveals in unprecedented detail circuit mechanisms of second-order conditioning. These mechanisms can explain the different properties of first- and second-order memories. They also provide a concrete example of how hierarchical interaction between dopamine subsystems contributes to a complex form of learning.

Results

Olfactory second-order conditioning following the odor-sugar association

As a prerequisite for mapping the underlying neuronal circuits and detailed characterization of memory properties, we established a robust protocol for appetitive second-order conditioning using a circular olfactory arena (Figure 1B and Figure 1-figure supplement 1; see Methods for our rationale for the selection of odors and other parameters). Flies were first trained to associate stimulus one (S1) odor with sugar and consolidated that memory for one day (Figure 1C). During second-order conditioning, 20 seconds of one S2 odor (S2+) was immediately followed by 10 seconds of the S1 odor, whereas another S2 odor (S2-) was presented alone. After five training sessions, flies increased their preference to the S2+ odor over the S2- odor when first-order

conditioning was long enough (i.e. 5 min; Figure 1D). This preference for the S2+ odor was not due to sensory preconditioning, another form of higher-order conditioning in which S2-S1 pairing was done *before* pairing S1-sugar (Figure 1E), although unimodal sensory preconditioning has been reported in aversive olfactory learning in *Drosophila* (Martinez-Cervantes et al., 2022).

First-order memory and its derived second-order memory exhibited marked differences in dynamics of formation and update. Second-order memory after odor-sugar conditioning did not last for one day and was susceptible to extinction (Figures 1F and G). With optogenetic stimulation of sugar sensory neurons, the first-order memory steadily increased during nine training sessions, whereas second-order memory peaked at the third training and declined subsequently (Figure 1H). This transiency of learning was not observed when activation of sugar sensory neurons was not omitted during second-order conditioning (Figure 1H). Learning of association between S2+ odor and activation of sugar sensory neurons was compromised when S2+ is preceded by S1 which predicts the occurrence of reward (Figure 1I). These results indicate that the transient and unstable nature of second-order memory observed across animal phyla also applies to *Drosophila*, and the temporal order of the stimuli is crucial for second-order conditioning as in first-order conditioning.

Identification of MB compartments that instruct second-order conditioning

To identify the circuit elements that might be particularly important for second-order conditioning, we examined whether first-order memory in certain MB compartments is more potent for instructing second-order conditioning than others. For this purpose, we substituted sugar with optogenetic activation of DANs to induce memory in a defined set of compartments (Figure 2A). Flies were first trained by pairing the S1 odor with optogenetic activation of specific DANs with CsChrimson

(see below for measurement of dopamine release). Then, the compartment-specific memory of the S1 odor was tested for its power as a reinforcer in second-order conditioning. Among four sets of DAN cell types that can induce first-order appetitive memory (Figure 2A), two sets — PAM-α1 and a combination of PAM-γ5 and β′2a — could induce significant second-order memory compared to the genetic control (Figure 2B). Similar to first-order conditioning, stimulus timing was an important factor for successful second-order conditioning (i.e. S2+ must precede S1; Figure 2C). PAM-α1 is known to be essential for learning nutritional value and is required for long-term appetitive memory (Yamagata et al., 2015), whereas memory induced by combinatorial activation of PAM-γ5 and PAM-β′2a is short-lasting (Aso and Rubin, 2016). As expected from those different stabilities of the first-order memory, memory in PAM-α1 but not PAM-γ5/β′2a could instruct second-order conditioning one day after the first-order conditioning (Figure 2B). Consistent with the outcome of this optogenetic experiment, blocking of synaptic transmission from PAM-α1 DANs with Tetanus Toxin (TNT) light chain abolished both S1 preference and second-order memory when assayed one day after odor-sugar conditioning (Figure 2D). In contrast, blocking PAM cluster DANs in the γ4, γ5, β′2a with TNT impaired the second-order conditioning without affecting S1 preference (Figure 2D). The second-order memory derived from the first-order memory in the α1 compartment exhibited the transient learning curve (Figure 2E-F) and susceptibility to extinction, recapitulating observations after odor-sugar conditioning (Figure 1F-H). Thus, these results suggest α1 as the primary candidate compartment to store the first-order memory that instructs second-order conditioning. The first-order memory in the γ5/β′2a compartments may have a supplemental contribution to second-order conditioning, especially shortly after the first-order conditioning.

Memory in α1 can instruct secondary plasticity across compartments

Memories and plasticity induced in different MB compartments differ in their properties including retention, induction threshold and resistance to extinction (Aso et al., 2012; Aso and Rubin, 2016; Hige et al., 2015; Huetteroth et al., 2015; Jacob and Waddell, 2020; Lin et al., 2014; Pai et al., 2013; Plaçais et al., 2013; Vrontou et al., 2021; Yamagata et al., 2015). The markedly distinct memory dynamics between first- and second-order memories noted above prompted us to hypothesize that those memories are formed in different MB compartments. For aversive memory, transient inactivation of MBON-γ1pedc (a.k.a MB-MVP2), which mimics the effect of synaptic depression caused by aversive learning, can serve as reinforcement (König et al., 2019; Ueoka et al., 2017). Thus, if our hypothesis is correct, and if the α1 compartment indeed is potent for instructing second-order conditioning, then local induction of synaptic plasticity in α1 should drive secondary plasticity in other compartments during second-order conditioning. Since PAM-γ5 and β′2a can induce robust appetitive memory that is short-lasting and susceptible to extinction (Figure 2A) (Aso and Rubin, 2016), we reasoned that second-order memory may involve compartments targeted by these DANs. To test this idea, we first generated a split-LexA driver to express ChrimsonR selectively in PAM-α1 (Figure 3 -figure supplement 1). We then labeled either MBON-α1 or MBON-γ5β′2a by split-GAL4 lines to make whole-cell recordings from them (Figures 3A and Figure 3 -figure supplement 2A). In MBON-α1, we found that pairing an odor and DAN activation leads to reduced spiking responses to that odor as in other MB compartments examined in previous studies (Figure 3-figure supplement 2) (Berry et al., 2018; Handler et al., 2019; Hige et al., 2015; Owald et al., 2015; Owald and Waddell, 2015; Séjourné et al., 2011; Vrontou et al., 2021). MBON-γ5β′2a, on the other hand, did not elicit action potentials that are readily distinguishable from synaptic potentials in response to odor presentation or current injection (Figure 3 -figure supplement 3). We therefore focused

on subthreshold responses. After a single round of second-order conditioning, MBON-γ5β′2a showed reduced responses to the S2+ odor, while responses to S2- did not change even after five repetitions of conditioning (Figures 3B and C). Repeated presentation of S2 odors without S1 did not cause a reduction of odor responses (Figures 3D and E). These results indicate that the α1 compartment can instruct second-order conditioning in the γ5/β′2a and potentially other compartments.

Candidate interneurons to mediate instruction signals for second-order conditioning

We next set out to identify the neuronal pathway responsible for the induction of second-order plasticity. MBON-α1 is the sole output pathway from the α1 compartment and is, like other reward memory compartment MBONs, glutamatergic. Glutamate functions as an inhibitory neurotransmitter with glutamate-gated-chloride channel (Liu and Wilson, 2013), although activity of glutamatergic MBONs can have a net excitatory effect on DANs via other receptors or indirect pathways (Cohn et al., 2015; Ichinose et al., 2015; Karuppudurai et al., 2014; Zhao et al., 2018). Upon induction of plasticity, MBON-α1's responses to learned odor will be depressed (Figure 3-figure supplement 2). Therefore, if glutamate is inhibitory, the downstream circuits of the MBON-α1 could gain an enhanced response to a learned odor as an outcome of reduced inhibition, could feed an excitatory drive to DANs for second-order conditioning, provided that there are such connections. However, α1 appears to be an exceptionally isolated compartment. MBON-α1 is the only MBON that does not send direct output to DANs innervating other compartments; rather it only directly connects with the DANs that innervate the same compartment, PAM-α1 (Figure 4-figure supplement 1A)(Li et al., 2020). Similarly, MBON-α1 shows very limited connections to DANs innervating other compartments that are mediated by a single interneuron (one-hop pathways; Li et al., 2020; Figure 4-figure

supplement 1B). This led us to explore pathways with two interneurons between MBON-α1 and DANs (two-hop pathways).

To explore pathways with interneurons between MBON-α1 and DANs, we queried the hemibrain EM connectome database (Li et al., 2020; Scheffer et al., 2020). We then used a pre-trained machine learning algorithm to predict the most likely neurotransmitters used by the connected neurons (Eckstein et al., 2020). Supplementary File 1 summarizes the full connection matrix, neurotransmitter predictions for the 396 major interneuron cell types with at least 100 total synapses with MBONs and DANs. In this way (see Methods for detail), we identified prominent cholinergic two-hop pathways from MBON-α1 to multiple reward-DANs including PAM-γ5, γ4, β′2a, β′2m, β′2p that were mediated by the interneurons SMP353/354 and SMP108 (Figure 4A; Figure 4-supplement 2). The SMP108 is an outstanding cell type in many features. Among all cholinergic neurons, SMP108 has the highest number of connections with reward DANs (Figure 4-figure supplement 3). SMP108 also synapses onto all three cholinergic interneurons (SMP177, LHPV5e1, LHPV10d1) in the second layer of the two-hop pathways, providing additional excitatory drive to PAM DANs (Figure 4B). Intriguingly, SMP108 also appeared as an outstanding cell type to receive direct inputs from MBON-γ5β′2a and output to DANs (Figure 4C). As discussed above, we identified the γ5/β′2a as additional compartments that, like α1, can instruct second-order memory. Taken together, among other candidate cell types such as CRE011 and LHPD5d1 (Figure 4C), the circuit centered at SMP108 appears to be a prominent candidate that converts first-order plasticity in both α1 and γ5β′2a compartments to excitatory drive to DANs.

Identification of SMP108 and its associated circuits allowed us to construct a few testable hypotheses regarding the circuit mechanisms of second-order conditioning. First, SMP108's response to the reward-predicting S1 odor should be potentiated after first-order conditioning. Second, activation of SMP108 should trigger dopamine release in the

MB compartments involved in appetitive memory. Third, the output of SMP108 should be required for second-order memory. Fourth, memory induced by the SMP108 pathway should recapitulate the transient and unstable nature of second-order memory. To experimentally test those hypotheses, we generated split-GAL4 drivers for SMP108 (SS67221 and SS45234; Figures 4D-F). Using these drivers, we confirmed that axonal terminals of SMP108 are immunoreactive to choline acetyltransferase (Figure 4E), which is consistent with the fact that 2,416 out of 2,753 presynaptic sites of SMP108 are predicted to be cholinergic in the hemibrain data (Supplementary File 1).

SMP108 acquires enhanced response to reward-predicting odor

First, we examined the change in SMP108's odor responses after pairing of an odor and optogenetic activation of PAM-cluster DANs, which can induce appetitive memory. As expected from the converging inputs from multiple lateral horn cell types (Supplementary File 1), SMP108 showed robust spiking responses to odors. After pairing, responses to the paired odor were selectively potentiated (Figure 5). Furthermore, reversal pairing de-potentiated the previously paired odor. Thus, SMP108 is capable of acquiring enhanced responses to S1 after first-order conditioning and flexibly tracking updates of odor-reward associations.

SMP108 evoked dopamine release in appetitive memory compartments

Next, we directly measured the pattern of dopamine release evoked by optogenetic activation of SMP108, its upstream neurons (SMP353 and SMP354), or DANs using a recently developed dopamine indicator DA2m (Sun et al., 2020). With direct stimulation of DANs, release of dopamine was largely restricted to the compartment(s) innervated by Chrimson-expressing DANs (Figure 6-figure supplement1). Consistent with EM connectivity, activation of SMP108 or SMP353/354 evoked dopamine release in the

303 reward memory compartments β′2, γ4 and γ5 compartments (Figure 6). SMP108
304 activation also evoked small dopamine release in β1 and β2, presumably via indirect
305 connections, but not in α1. Notably, we observed that the dopamine signal in γ2, which
306 is tuned to punitive stimuli, was significantly reduced after SMP108 activation (Figure 6-
307 figure supplement 1C). Other DANs for aversive memories such as PAM-γ3, PPL1-
308 γ1pedc, and PPL1-α3 showed very weak response, if any. Thus, activation of SMP108
309 triggers dopamine release selectively in multiple reward memory compartments.
310
311 **SMP108 is required for second-order conditioning**
312 As expected from above results, we found that blocking neurotransmission of SMP108
313 by expression of TNT using two different split-GAL4 drivers impaired second-order
314 conditioning compared to genetic controls (Figure 7A). We were unable to block
315 SMP108 only during the second-order conditioning using the thermogenetic effector
316 shibire^{ts1} because flies with control genotype rapidly extinguished the first-order memory
317 and failed to perform second-order conditioning at the 32℃ restrictive temperature (data
318 not shown). Nonetheless, blocking SMP108 with TNT did not impair the first-order
319 memory with 2min or 1-day retention (Figure 7B), indicating that flies with blocked
320 SMP108 were fully capable of smelling odors, tasting sugar, and forming, consolidating,
321 and retrieving the first-order appetitive memory.
322 To further assess the potential contribution of SMP108 to appetitive memory
323 retrieval, we tested whether activation of SMP108 triggers any relevant behavior. Flies
324 steer to an upwind orientation in the presence of reward-predicting odors and food-
325 related odors like vinegar (Álvarez-Salvado et al., 2018; Borst and Heisenberg, 1982;
326 Handler et al., 2019). Upon optogenetic stimulation of SMP108 with CsChrimson, flies
327 indeed changed their mean orientation and walked upwind in the same circular arena
328 used in the olfactory conditioning experiments described above (Figure 7-figure

supplement 1A). However, we did not observe any impairment of upwind steering in response to the sugar-associated odor in SMP108-blocked flies (Figure 7-figure supplement 1B), suggesting the existence of redundant circuits that trigger memory-based upwind steering. Thus, SMP108 could contribute to retrieval of reward memory for guiding actions, but its requirement is limited to second-order conditioning. Taken together, these results indicate that SMP108, which we identified as a prominent anatomical hub for the feedforward circuit between reward memory compartments, indeed plays a key role in second-order conditioning by triggering dopamine signals in response to the reward-predicting cue.

SMP108 pathway induces transient memory

Based on the results so far, we propose a teacher-student compartment model that explains the induction mechanism of second-order memory and its distinct dynamics from first-order memory (Figure 8A). In this model, local plasticity induced in a stable memory compartment (i.e. α1) during first-order conditioning functions as a reinforcer to induce secondary plasticity in other transient memory compartments through interneurons (i.e. SMP108) that connect those memory compartments. Thus, this model predicts that target compartments of SMP108 pathway collectively express transient memory dynamics that recapitulates unstable nature of second-order memory induced by sugar-odor (Figures 1F and 1G) or optogenetic conditioning (Figures 1H, 2E and 2G).

To test this prediction, we next examined the dynamics of memory induced by the SMP108 pathway in detail and compared them to those induced by direct stimulation of PAM-α1 and other DAN types using CsChrimson (Figures 8B and Figure 8-figure supplement 1). The protocol started by assessing naïve odor preference that was designed to be canceled by reciprocal experiments. Then flies were sequentially trained five times by 10s, 30s, 60s, 60s and 60s periods of odor presentation paired with LED

activation, and then another odor presented without LED activation (training phase). Memory was tested by giving a choice between odors after each training. After the fifth training, memory was tested 12 times without pairing with LED activation (extinction phase). Then flies were trained with a reversal protocol 5 times and tested 12 times (reversal phase). After one more round of reversal phase (re-reversal), flies were exposed to LED activation without odor to test the susceptibility of memory to non-contingent activation of DANs, a protocol that is known to erase memory (Berry et al., 2012; Plaçais et al., 2012). These experiments revealed that memories induced by SMP108 or its upstream SMP353/354 differ in several ways from the memory induced by activation of PAM-α1 (Figure 8C-F). First, SMP108 and SMP353/354 can induce memory more rapidly than PAM-α1 (Figure 8C). Second, memories formed by SMP108 and SMP353/354 declined during later training sessions and during the extinction phase, whereas memory formed by PAM-α1 remained high (Figure 8D and E). Third, memory formed by PAM-α1 was resistant to DAN activation, but memories formed by SMP108 and SMP353/354 were decreased (Figure 8F). Such transient learning and fast extinction are reminiscent of second-order conditioning by sugar (Figures 1F and 1G) or optogenetics (Figures 1H, 2E, and 2G). In contrast to the activation of CsChrimson in PAM-α1, drivers that target CsChrimson to SMP108's downstream DANs exhibited memory dynamics similar to those observed when CsChrimson is activated in SMP108 or SMP353/354. For instance, MB032B and MB213B split-GAL4 that target CsChrimson in β′2m and β1/β2, respectively, induced transient memories (Figure 8E). Consistent with this, fitting the memory dynamics formed by SMP108 with a linear sum of direct DAN activation data indicated an overweight of MB032B (β′2m), MB213B (β1/β2) and MB312C (γ4), and zero weight for MB043C (α1) (Figure 8G). However, the high memory score of SMP108 activation after the first 10s training was fitted poorly, indicating that combinatorial activation of DANs and/or suppression of DANs innervating γ2 (Figure 6-

figure supplement 1C) might have a synergistic effect on memory formation. These experiments highlight the distinct memory properties exhibited by upstream and downstream partners of SMP108, and might help explain the circuit mechanisms underlying the difference between first- and second-order memories.

Discussion

In this study, we used the *Drosophila* mushroom body as a model system to examine how multiple dopamine-driven memory circuits interact to enable second-order conditioning. Although second-order conditioning has been demonstrated behaviorally in many species, there is little circuit-level knowledge to provide mechanistic insight. By developing a robust appetitive second-order conditioning protocol and utilizing the EM connectome map in *Drosophila*, we uncovered neural circuit mechanisms that define dynamics and learning rules of second-order conditioning.

Origins of the unique learning rules of second-order conditioning

Our optimization of the second-order conditioning protocol using actual sugar reward or its optogenetic substitution revealed important properties of second-order memory and enabled detailed circuit interrogation. Formation of second-order memory was most effective either when the first-order S1 odor predicted a strong sugar reward (Figure 1D) or when long-term first-order memory was optogenetically induced (Figure 2B). Furthermore, during second-order training following optogenetic first-order conditioning, S2 odor must precede the S1 odor (Figure 2C). With additional second-order training sessions, second-order memory could become as robust as the first-order memory, but the continual omission of the expected fictive reward during training and extinction trials tended to reduce second-order memory (Figures 1H, 2E, and 2G). The retention of second-order

memory was also shorter than first-order memory when we used actual sugar reward for first-order conditioning (Figure 1F). Remarkably, all the dynamics and learning rules we found in *Drosophila* for second-order conditioning are well-conserved across animal phyla (Gewirtz and Davis, 2000; Pavlov, 1927; Rescorla, 1980). Our study indicates that, in flies, at least some of these phenomena can be accounted for by the teacher-student model of the MB circuit, which hypothesizes distinct dynamics of plasticity in individual compartments and hierarchical interactions between compartments. Namely, a compartment with a slow learning rate instructs compartment(s) with transient memory dynamics.

Requirement of long first-order training for successful formation of second-order memory (Figure 1C and D) can be explained by the properties of the α1, which we identified as the teacher compartment. The DANs in α1 respond to sugar relatively weakly compared to other DANs in the β′2, β2, γ4, γ5 compartments (Siju et al., 2020). Also the α1 compartment exhibited the slowest learning rate of all compartments even with optogenetic stimulation of DANs that efficiently release dopamine (Figure 6-figure supplement 1 and Figure 8C). Once established, however, memory in the α1 is highly resistant to extinction (Figures 2A and 8D), which is likely critical for forming second-order conditioning without compromising first-order memory. These considerations emphasize the eligibility of the α1 compartment as a teaching compartment among all reward-memory compartments. On the other hand, transient and unstable nature of second-order memory can be ascribed to collective properties of student compartments (Figure 8). Future studies are required to identify intrinsic molecular factors and microcircuit elements responsible for distinct dynamics of teacher and student compartments.

Implications to the higher-order functions of heterogeneous dopamine subsystems

Our study identified a role of hierarchical interaction between dopamine-based memory subsystems. Importantly, heterogeneous populations of DANs are also found in vertebrate species, and they are involved in distinct types of learning. Studies using visual conditioning in monkeys found that distinct types of DANs projecting to the head or tail regions of the caudate nucleus change their response to reward-predicting cues with very different dynamics (Kim et al., 2015, 2014). A recent study in rodents indicated that subsets of DANs have diverse learning rates to compute positive and negative reward prediction errors to enable distributional reinforcement learning (Dabney et al., 2020). Cue-evoked dopamine transients at the onset of reward-predicting cues are required for second-order conditioning in rodents (Maes et al., 2020). Such dopamine transients could be derived from memory encoded by the same DAN, other type(s) of DANs, or both, depending on the architecture of feedback circuits. Given the conserved nature of second-order memory transiency across animal phyla, future studies in vertebrate models may also reveal a hierarchical interaction between dopamine cell types with fast and slow dynamics in second-order conditioning.

Second-order conditioning is merely one example of learning that depends on higher-order connections between dopamine-dependent memory subsystems. In fact, in flies, feedback and feedforward connections between MBONs and DANs or lateral connections between MBONs are implicated in extinction of aversive and appetitive memory as well as consolidation of memories (Felsenberg et al., 2018, 2017; McCurdy et al., 2021). The EM connectome map, along with computational modeling (Gkanias et al., 2022; Jiang and Litwin-Kumar, n.d.), will guide further investigation of intercompartmental interactions. For instance, we identified one outlier cell type of GABAergic interneuron LHCENT3 that receives inputs from glutamatergic MBON-γ5β′2a and outputs to reward DANs (Figure 4C). This cell type may serve as the substrate for subtraction of expected reward in the computation of reward prediction error, as GABAergic neurons in VTA do in

vertebrate brains (Starkweather and Uchida, 2021). Although the majority of circuit-level research has focused on rather simple forms of learning that involve primary reinforcers, animals have abundant opportunities to shape their behaviors through indirect learning that depends on existing memory. We expect that network motifs similar to what we identified here contribute to various forms of such complex learning. We expect that future modeling studies constrained by the EM connectome and large scale behavioral and neural activity data will lead to a comprehensive understanding of the MB's contributions to these computations.

Contents of second-order conditioning

Understanding what is learned is a fundamental challenge in studies of associative learning. There are many possible structures of associations that would allow animals to perform second-order conditioning tasks. Our finding of the cross-compartmental nature of second-order conditioning makes it unlikely that flies associate S2 with a *specific* type of reward used as US, because individual MB compartments are tuned to different kinds of rewards or reward responses. That is, while DANs in the teacher compartment α1 are essential for nutritional value learning (Yamagata et al., 2015), those in the student compartments γ4 and β′2 respond to water in thirsty flies (Lin et al., 2014). DANs in γ4, γ5 and β′2 also represent vinegar and activity of DANs in γ4 correlates with upwind steering (Lewis et al., 2015; Zolin et al., 2021). DANs in β′2a also respond to a punishment-predicting odor when punishment is omitted (McCurdy et al., 2021). Thus, based on our circuit mapping and the known functions of the relevant circuits, we propose that S2 is associated with positive valence that was originally associated with S1 but generalized to broader types of rewards. This view is consistent with the fact that second-order conditioning is typically insensitive to subsequent reduction of the value of the US (i.e. devaluation), which suggests that an association is formed between S2 and the original

valence of the US rather than the US itself (Rescorla, 1980). Studies in rodents demonstrated that S1 and S2 with different sensory modalities can elicit distinct conditioned responses (CRs), supporting the idea that S2 is not associated with the specific CR elicited by S1 (Holland, 1977; Kim et al., 1996). Notably, a broadening of the category of expected rewards in second-order conditioning has been suggested by a study in pigeons (Stanhope, 1992), where differential CRs to qualitatively distinct USs (i.e. food and water) were observed for S1 but not for S2. Thus, our circuit underpinning of second-order conditioning provides a concrete neuronal substrate for behavioral and psychological phenomena that have been described for decades.

Materials and Methods

Fly strains

Drosophila melanogaster strains were reared at 22C and 60% humidity on standard cornmeal food in 12:12 hour light:dark cycle. 4-10 days of adult females were used 2-4 days after sorting them on the Peltier cold plate. For flies expressing Chrimson (Klapoetke et al., 2014) the food was supplemented with retinal (0.2 mM all-trans-retinal prior to eclosion and then 0.4 mM). Driver and effector lines are listed in the key resource table and genotypes used by each figure are listed below. The new collection of split-GAL4 and split-LexA drivers was designed based on confocal image databases (http://flweb.janelia.org) (Jenett et al., 2012), and screening expression patterns of p65ADZp and ZpGAL4DBD combinations as described previously (Aso et al., 2014; Pfeiffer et al., 2010). Confocal stacks of new split-GAL4 driver lines used in this study are available at http://www.janelia.org/split-gal4.

Detailed fly genotypes used by figures

Figure	Genotype
Figure 1C-G, Figure 1-figure supplement 1	*Canton S*
Figure 1H	*w/w, 20xUAS-CsChrimson-mVenus attP18;+/Gr64f-GAL4;+/Gr64f-GAL4*
Figure 2A-C	*w/w, 20xUAS-CsChrimson-mVenus attP18;;+/MB043C-split-GAL4* *w/w, 20xUAS-CsChrimson-mVenus attP18;+/MB213B-split-GAL4* *w/w, 20xUAS-CsChrimson-mVenus attP18;;+/MB312C-split-GAL4* *w/w, 20xUAS-CsChrimson-mVenus attP18;MB109B/MB315C-split-GAL4* *w/w, 20xUAS-CsChrimson-mVenus attP18;+/ Empty-split-GAL4*
Figure 2D	*w/+;Empty-split-GAL4/UAS-TNT (II)* *w/+;MB196B/UAS-TNT (II)* *w/+;MB043C/UAS-TNT (II)*
Figure 3 Figure 3-figure supplement 3	*w/w,13XLexAop2-IVS-ChrimsonR-mVenus-p10 attP18, 20XUAS-syn21 mScarlet-opt-p10 su(Hw)attp8; SS01308-split-GAL4/MB043-split-LexA*
Figure 3-figure supplement 1	*w/w,13XLexAop2-IVS-ChrimsonR-mVenus-p10 attP18, 20XUAS-syn21 mScarlet-opt-p10 su(Hw)attp8; +/MB043-split-LexA* *w/w,13XLexAop2-IVS-ChrimsonR-mVenus-p10 attP18, 20XUAS-syn21 mScarlet-opt-p10 su(Hw)attp8; MB319C-split-GAL4/MB043-split-LexA* *w/w,13XLexAop2-IVS-ChrimsonR-mVenus-p10 attP18, 20XUAS-syn21 mScarlet-opt-p10 su(Hw)attp8; SS01308-split-GAL4/MB043-split-LexA* *w/w,13XLexAop2-IVS-ChrimsonR-mVenus-p10 attP18, 20XUAS-syn21 mScarlet-opt-p10 su(Hw)attp8; SS67221-split-GAL4/MB043-split-LexA*
Figure 3-figure	*w/w,13XLexAop2-IVS-ChrimsonR-mVenus-p10 attP18, 20XUAS-syn21 mScarlet-opt-p10 su(Hw)attp8; MB319C-split-*

supplement 2	*GAL4/MB043-split-LexA*
Figure 4E	*w/w, pJFRC200-10xUAS-IVS-myr::smGFP-HA in attP18; pJFRC225-5xUAS-IVS-myr::smGFP-FLAG in VK00005/SS67221-split-GAL4*
Figure 4F	*pBPhsFlp2::PEST in attP3;; pJFRC201-10XUAS-FRT>STOP>FRT-myr::smGFP-HA in VK0005, pJFRC240-10XUAS-FRT>STOP>FRT-myr::smGFP-V5-THS-10XUAS-FRT>STOP>FRT-myr::smGFP-FLAG in su(Hw)attP1/SS67221-split-GAL4*
Figure 5	*13XLexAop2 IVS p10 ChrimsonR mVenus trafficked in attP18/+; 58E02-LexAp65 in attP40/ VT026646-p65ADZp in attP40 (ss45234-split); pJFRC28-10XUAS-IVS-GFP-p10 in su(Hw)attP1 / VT029309-ZpGdbd in attP2 (ss45234-split)*
Figure 6, Figure 6-figure supplement 1	*w/w, 10XUAS-Chrimson88-tdTomato attP18; 13F02-LexAp65 attP40; LexAop2-DA2m VK00005/MB043C-split-GAL4* *w/w, 10XUAS-Chrimson88-tdTomato attP18; 13F02-LexAp65 attP40; LexAop2-DA2m VK00005/MB213B-split-GAL4* *w/w, 10XUAS-Chrimson88-tdTomato attP18; 13F02-LexAp65 attP40; LexAop2-DA2m VK00005/MB032B-split-GAL4* *w/w, 10XUAS-Chrimson88-tdTomato attP18; 13F02-LexAp65 attP40; LexAop2-DA2m VK00005/MB109B-split-GAL4* *w/w, 10XUAS-Chrimson88-tdTomato attP18; 13F02-LexAp65 attP40; LexAop2-DA2m VK00005/MB315C-split-GAL4* *w/w, 10XUAS-Chrimson88-tdTomato attP18; 13F02-LexAp65 attP40; LexAop2-DA2m VK00005/MB312C-split-GAL4* *w/w, 10XUAS-Chrimson88-tdTomato attP18; 13F02-LexAp65 attP40; LexAop2-DA2m VK00005/SS33917-split-GAL4* *w/w, 10XUAS-Chrimson88-tdTomato attP18; 13F02-LexAp65 attP40; LexAop2-DA2m VK00005/SS67221-split-GAL4*
Figure 7	*w/+;SS67221/+* *w/+; SS67221/UAS-TNT (II)* *w/+;SS45234/+* *w/+; SS45234/UAS-TNT (II)* *w/+;Empty-split-GAL4/TNT (II)SS67221/TNT*
Figure 7-figure supplement 1A	*w/w, 20xUAS-CsChrimson-mVenus attP18;+/ Empty-split-GAL4* *w/w, 20xUAS-CsChrimson-mVenus attP18;+/SS67221-split-GAL4*
Figure 7-figure supplement 1B	*w/+;SS67221/+* *w/+; SS67221/UAS-TNT (II)* *w/+;Empty-split-GAL4/TNT (II)SS67221/TNT*
Figure 8, Figure 8-figure supplement 1	*w/w, 20xUAS-CsChrimson-mVenus attP18;+/+;+/MB043C-split-GAL4* *w/w, 20xUAS-CsChrimson-mVenus attP18;+/SS33917-split-GAL4* *w/w, 20xUAS-CsChrimson-mVenus attP18;+/SS67221-split-GAL4* *w/w, 20xUAS-CsChrimson-mVenus attP18;+/MB032B-split-GAL4* *w/w, 20xUAS-CsChrimson-mVenus attP18;+/MB109B-split-GAL4* *w/w, 20xUAS-CsChrimson-mVenus attP18;+/+;+/MB315C-split-GAL4* *w/w, 20xUAS-CsChrimson-mVenus attP18;+/MB312C-split-GAL4* *w/w, 20xUAS-CsChrimson-mVenus attP18;+/MB213B-split-GAL4*

Olfactory conditioning

Olfactory conditioning was performed as previously described (Aso et al., 2016). Groups of approximately 20 females of 4–10 d post-eclosion were trained and tested using the modified four-field olfactory arena (Aso and Rubin, 2016; Pettersson, 1970) equipped with the 627nm LED board (34.9 μW/mm2 at the position of the flies) and odor mixers. The flow rate of input air from each of the four arms was maintained at 100 mL/min throughout the experiments by mass-flow controllers, and air was pulled from the central hole at 400 mL/min. Odors were delivered to the arena by switching the direction of airflow to the tubes containing diluted odors using solenoid valves. The odors were diluted in paraffin oil: 3-octanol (OCT 1:1000), 4-methylcyclohexanol (MCH; 1:750), Pentyl acetate (PA: 1:10000) and ethyl lactate (EL: 1:10000). Sugar conditioning was performed by using tubes with sucrose absorbed Whatman 3 MM paper as previously described (Krashes and Waddell, 2008; Liu et al., 2012). Before conditioning, flies were starved for 40-48 hour on 1% agar. Videography was performed at 30 frames per second and analyzed using Fiji. For experiments with one day retention, flies were kept in agar vials at 21C after first-order conditioning. For testing olfactory memories, distribution of flies in four quadrants were measured for 60 s. The performance index (PI) is defined as a mean of [(number of flies in the two diagonal quadrants filled the one odor) - (number of flies in other two quadrants filled with another odor or air)]/(total number of flies) during final 30 s of 60 s test period. The average PI of reciprocal experiments is shown in figures to cancel out potential position bias and innate odor preference. Although genotypes of flies were not hidden to experimentalists, handling was minimized by automation of stimulus delivery. We included all the data if experiments were validated by metadata such as airflow readout from the mass flow controllers.

Optimization of second-order conditioning

To establish a training protocol for robust olfactory second-order conditioning in *Drosophila*, we first characterized how innate preference for an odor (when compared with pure air) changes over multiple trials using the four-armed olfactory arena (Figure-figure supplement 1)(Aso and Rubin, 2016; Pettersson, 1970). We previously chose concentrations of two conventional odors, 4-methylcyclohexanol (MCH) and 3-octanol (OCT), so that naïve fed flies show behavioral responses to each odor at a similar level, minimizing bias between them (Tully and Quinn, 1985). At the same concentration, starved flies showed slight attraction to the MCH at the first trial, then gradually shifted to aversion in subsequent trials (Figure 1-figure supplement 1). In contrast, both fed and starved flies showed aversion to the OCT, which gradually decreased in subsequent trials. Because the innate aversiveness of OCT may preclude appetitive second-order conditioning, we decided to use MCH as the first conditioned stimulus (S1) throughout this study.

The strength of second-order conditioning tends to be low, compared to that of first-order, but can be enhanced by using an unconditioned stimulus (US) of high intensity and sensory stimuli within the same modality (Helmstetter and Fanselow, 1989; Rescorla and Furrow, 1977). Thus, we examined the effect of increasing conditioning duration. After pairing MCH with sugar for increasing durations (0, 2, 5 min), flies were allowed to consolidate the memory for one day. Then the stability of first-order memory was tested by repeating binary choice between S1 odor and air for 12 times. All trained flies showed attraction to MCH during at least the first five trials (Figure 1C). One 2-min training was enough to induce appetitive memory (Krashes and Waddell, 2008; Tempel et al., 1983), but longer 5-min training resulted in slightly stronger memories during the first five tests on average. Therefore, we decided to limit the number of second order conditioning to five times. We used two odorants, pentyl acetate (PA) and ethyl lactate (EL) as the second conditioned stimuli (S2). These odors are known to evoke discrete patterns of activity in Kenyon cells (Campbell et al., 2013) and thought to be easily discriminated against. Innate behavioral responses to these odors were relatively stable over 12 trials (Figure 1-figure supplement 1).

For first-order conditioning, flies learn best when sensory cues precede US or DAN activation (Aso and Rubin, 2016; Tanimoto et al., 2004). Thus, during second-order conditioning, 20 seconds of one S2 odor (S2+) was immediately followed by 10 seconds of the S1 odor, whereas another S2 odor (S2-) was presented alone. Flies failed to form second-order memory when S1 preceded S2+ (Figure 2C). PA and EL were S2+ and S2- odors, respectively, in half of a set of reciprocal experiments. The S2+ and S2- odors were swapped in the other half of reciprocal experiments. After five training sessions, unpaired control flies showed weak attraction to S2+, possibly due to innate attractiveness of MCH in starved flies (Figure 1-figure supplement 1). Compared to this basal response, flies preferred the S2+ odor over the S2- odor when first-order conditioning was long enough (i.e. 5min; Figure 1D). This preference for the S2+ odor was not due to stimulus generalization of S1 (MCH) to PA or EL, because such bias is designed to be canceled by our experimental design involving reciprocal experiments. Both immediate and one-day first-order memories were potent to induce second-order memory, but second-order memory did not last for one day (Figure 1F.

Response Airflow

For testing airflow directional response, we used the same circular olfactory arena (Figure 7-figure supplement 1), in which air flows from peripheral to a hole at the center. Each fly's distance from center (r_i) was measured and area normalized index (r_i/r_{arena})*(r_i/r_{arena}) was calculated. r_{arena} is the radius of the arena. When flies distribute randomly in the arena, mean r is 1/sqrt(2) and area normalized index is 1/2. To calculate upwind displacement, the mean of arena normalized distance from center at each time point in each movie was subtracted by that at the onset of LED or odor.

Electrophysiology

Fly stocks for electrophysiological experiments were maintained at room temperature on conventional cornmeal-based medium (Archon Scientific). Experimental flies were collected on the day of eclosion, transferred to all-trans-retinal food (0.5 mM) and kept in the dark for 48-72 hr. For second-order conditioning experiments, flies were starved for 60-72 hr after feeding retinal food.

In vivo whole-cell recordings were performed as previously reported (Hige et al., 2015). The patch pipettes were pulled for a resistance of 4-6MΩ and filled with pipette solution containing (in mM): L-potassium aspartate, 140; HEPES, 10; EGTA, 1.1; $CaCl_2$, 0.1; Mg-ATP, 4; Na-GTP, 0.5 with pH adjusted to 7.3 with KOH (265 mOsm). The preparation was continuously perfused with saline containing (in mM): NaCl, 103; KCl, 3; $CaCl_2$, 1.5; $MgCl_2$, 4; $NaHCO_3$, 26; N-tris(hydroxymethyl) methyl-2-aminoethane-sulfonic acid, 5; NaH_2PO_4, 1; trehalose, 10; glucose, 10 (pH 7.3 when bubbled with 95% O_2 and 5% CO_2, 275 mOsm). For recordings from starved flies, trehalose and glucose were replaced by equimolar sucrose. Whole-cell recordings were made using the Axon MultiClamp 700B amplifier (Molecular Devices). Target cells were visually targeted by fluorescence signal with a 60X water-immersion objective (LUMPlanFI/IR; Olympus) attached to an upright microscope (OpenStand; Prior Scientific). Cells were held at around -60 mV by injecting hyperpolarizing current, which was typically < 100 pA. Signals were low-pass filtered at 5 kHz and digitized at 10 kHz.

For odor delivery, a previously described custom-designed device was used (Hige et al., 2015). Saturated head space vapors of pure chemicals were air-diluted to 0.5 % (for second-order conditioning) or 2% (for the other experiments) before being presented to flies. Photostimulation was delivered by a high-power LED source (LED4D067; Thorlabs) equipped with 625 nm LED. Light pulses controlled by an LED driver (DC4100; Thorlabs) were presented to the brain at 17 mW/mm^2 through the objective lens.

Data acquisition and analyses were done by custom scripts in MATLAB (MathWorks). Instantaneous spike rates were calculated by convolving spikes with a Gaussian kernel (SD = 50 ms). Subthreshold odor responses and odor-evoked spikes were calculated with the time window of 1.2 s (for 1-s odor presentation) or 20.6 s (for 20-s odor presentation) from odor onset. Spontaneous spikes were subtracted to calculate odor-evoked spikes.

Dopamine imaging

Virgin females of *10XUAS-Chrimson88-tdTomato attP18; R13F02-LexAp65 in attP40;LexAop2-DA2m in VK00005* (Klapoetke et al., 2014; Sun et al., 2020) were crossed with split-GAL4 driver lines, and progenies were reared at 25 ℃ on retinal supplemented (0.2 mM) cornmeal medium that was shielded from light. All experiments were performed on female flies, 3-7 days after eclosion. Brains were dissected in a saline bath (103 mM NaCl, 3 mM KCl, 2 mM CaCl2, 4 mM MgCl2, 26 mM NaHCO3, 1 mM NaH2PO4, 8 mM trehalose, 10 mM glucose, 5 mM TES, bubbled with 95% O2 / 5% CO2). After dissection,

the brain was positioned anterior side up on a coverslip in a Sylgard dish submerged in 3 ml saline at 20℃. The sample was imaged with a resonant scanning 2-photon microscope with near-infrared excitation (920 nm, Spectra-Physics, INSIGHT DS DUAL) and a 25× objective (Nikon MRD77225 25XW). The microscope was controlled using ScanImage 2016 (Vidrio Technologies). Images were acquired over a 231 µm × 231 µm x 42 µm volume with a step size at 2 µm. The field of view included 512 × 512 pixel resolution taken at approximately 1.07 Hz frame rate. The excitation power during imaging was 19 mW.

For the photostimulation, the light-gated ion channel CsChrimson was activated with a 660-nm LED (M660L3 Thorlabs) coupled to a digital micromirror device (Texas Instruments DLPC300 Light Crafter) and combined with the imaging path with a FF757-DiO1 dichroic (Semrock). On the emission side, the primary dichroic was Di02-R635 (Semrock), the detection arm dichroic was 565DCXR (Chroma), and the emission filters were FF03-525/50 and FF01-625/90 (Semrock). An imaging session started with a 30 s baseline period, followed by a 1 s stimulation period when 12 µW/mm2 photostimulation light was delivered, and responses were detected over a 30 s post stimulation period. This was repeated for 10 trials. The light intensity was measured using the Thorlabs S170C power sensor.

For quantification of dopamine sensor signals, we used custom python scripts to draw ROIs corresponding to mushroom body compartments on maximum intensity projection over time. Before calculating the change in fluorescence (ΔF), fluorescence from a background ROI was subtracted. The background ROI was drawn in a region with no fluorescence. Baseline fluorescence is the mean fluorescence over a 30 s time period before stimulation started. The ΔF was then divided by baseline to normalize signal (ΔF/F). The mean responses from the 10 trials were calculated for each animal (4-6 samples per driver). Kruskal-Wallis H (KW) test was used for multi-comparison. Post-hoc pairwise comparison was made with the Wilcoxon rank-sum test.

Connectivity analysis

For producing the connectivity data shown in Figures 4 and Figure 4-figure supplement 1-3, connectivity information was retrieved from neuPrint (neuprint.janelia.org) hosting the "hemibrain" dataset (Scheffer et al., 2020), which is a publicly accessible web site (https://doi.org/10.25378/janelia.12818645.v1). For cell types, we cited cell type assignments reported in Sheffer et al., 2020. Only connections of the cells in the right hemisphere were used due to incomplete connectivity in the left hemisphere (Zheng et al., 2018). Connectivity data was then imported to a software Cytoscape (https://cytoscape.org/) for generating the diagrams before finalizing on Illustrator. The 3D renderings of neurons presented were generated using the visualization tools of NeuTu (Zhao et al., 2018) or VVD viewer (https://github.com/takashi310/VVD_Viewer; (Wan et al., 2012).

Neurotransmitter prediction

The method for neurotransmitter prediction using electron microscopy images and a 3D VGG-style network were described in detail for the FAFB data of a whole fly brain (Eckstein et al., 2020; Zheng et al., 2018). We used the same approach to train the network to classify individual presynaptic sites of FIB-SEM hemibrain data into the same six major neurotransmitters in fly brains as for FAB, i.e.: GABA, glutamate, acetylcholine, serotonin, dopamine and octopamine. Due to the differences in resolution between FAFB and the electron microscopy images used here, we adapted the architecture of the 3D VGG network to be isotropic as follows: We use four downsampling layers with uniform pooling

sizes of 2x2x2 on 3D crops centered on synapses with a side-length of 80 voxels. The results for 396 major interneurons are summarized in Supplementary File 1.

Immunohistochemistry

Brains and ventral nerve cord of 4-10 days old female were dissected, fixed and immunolabeled as previously described using the antibodies listed in the Key Resource Table (Aso et al., 2014; Nern et al., 2015). Samples were imaged with confocal microscopes (Zeiss LSM710, LSM780 or LSM880). Inset images in Figure 4E were taken with Airyscan.

Regression analysis of SMP108 memory dynamics

For each strain, the log-probability ratio of reinforced vs. unreinforced stimuli was computed as $R = log(p/(1-p))$, where p is the probability of choosing the reinforced stimulus. To relate the memory dynamics induced by SMP108 to those induced by DANs that it activates, we performed non-negative linear least-squares regression of the log-probability ratio for SMP108 against the ratios for PAM DANs. This reflects an assumption that the combinatorial activation of multiple compartments contributes a behavioral bias that is additive in log-probability ratio.

Statistics

Statistical comparisons were performed on GraphPad Prism or MATLAB using the Kruskal Wallis test followed by Dunn's post-test for multiple comparison, t-tests, or two-way ANOVA followed by Tukey's post hoc multiple comparisons test designated in figure legends. Non-parametric test was preselected for behavioral assays due to expected lack of normality or equal variance in subsets of data. Sample size was not predetermined based pilot experiments.

Data availability

The confocal images of expression patterns are available online (http://www.janelia.org/split-gal4). The source data for each figure are included in the manuscript.

Supplemental information

Supplementary File 1 Neurotransmitter prediction and a full connection matrix for MBONs, DANs and 396 interneurons cell types.

Numbers in column B-G are numbers of presynaptic sites that are predicted to be designated neurotransmitters. EM id in column K is an identification number in EM hembrain data. The other columns are the connection matrix. Top row indicates the direction of connections. For instance, 153 in the raw 5 of column M indicate the number of connections from MBON01 to SMP108, while 166 in the raw5 of column BD indicate the number of connections from SMP108 to PAM02. For the cell type consisting of multiple cells, a summed number of connections are shown.

Appendix

Key Resource Table

Acknowledgments

We thank Daisuke Hattori, James Fitzgerald, Sandro Romani, Gerald M. Rubin, Yichun Shuai, Mehrab Modi, Zongwei Chen, Adithya Rjagopalan and members of the Y.A. and T.H. labs for valuable discussion and comments on the manuscript. We thank Jinyan Liu and all the members of Janelia Flylight, jET, fly facility and scientific computing for construction of behavioral setup, generation and confocal microscopy images of split-GAL4 drivers. D.Y. was supported by Toyobo Biotechnology Foundation Postdoctoral Fellowship and Japan Society for the Promotion of Science Overseas Research Fellowship. Y.A. was supported by HHMI. T.H. was supported by NIH (R01DC018874), NSF (2034783), BSF (2019026) and UNC Junior Faculty Development Award. A.L.-K. was supported by the Burroughs Wellcome Foundation, the Gatsby Charitable Foundation, the McKnight Endowment Fund, the Simons Collaboration on the Global Brain, NIH award R01EB029858, and NSF award DBI-1707398.

Competing interests

The authors declare no competing interests.

References

Álvarez-Salvado E, Licata AM, Connor EG, McHugh MK, King BM, Stavropoulos N, Victor JD, Crimaldi JP, Nagel KI. 2018. Elementary sensory-motor transformations underlying olfactory navigation in walking fruit-flies. *Elife* **7**. doi:10.7554/eLife.37815

Aso Y, Hattori D, Yu Y, Johnston RM, Iyer NA, Ngo T-TB, Dionne H, Abbott LF, Axel R, Tanimoto H, Rubin GM. 2014. The neuronal architecture of the mushroom body provides a logic for associative learning. *Elife* **3**:e04577.

Aso Y, Herb A, Ogueta M, Siwanowicz I, Templier T, Friedrich AB, Ito K, Scholz H, Tanimoto H. 2012. Three dopamine pathways induce aversive odor memories with different stability. *PLoS Genet* **8**:e1002768.

Aso Y, Ray RP, Long X, Bushey D, Cichewicz K, Ngo T-T, Sharp B, Christoforou C, Hu A, Lemire AL, Tillberg P, Hirsh J, Litwin-Kumar A, Rubin GM. 2019. Nitric oxide acts as a cotransmitter in a subset of dopaminergic neurons to diversify memory dynamics. doi:10.7554/eLife.49257

Aso Y, Rubin GM. 2016. Dopaminergic neurons write and update memories with cell-type-specific rules. *Elife* **5**. doi:10.7554/eLife.16135

Avarguès-Weber A, Chittka L. 2014. Observational conditioning in flower choice copying by bumblebees (Bombus terrestris): influence of observer distance and demonstrator movement. *PLoS One* **9**:e88415.

Berry JA, Cervantes-Sandoval I, Chakraborty M, Davis RL. 2015. Sleep Facilitates Memory by Blocking Dopamine Neuron-Mediated Forgetting. *Cell* **161**:1656–1667.

Berry JA, Cervantes-Sandoval I, Nicholas EP, Davis RL. 2012. Dopamine is required for learning and forgetting in Drosophila. *Neuron* **74**:530–542.

Berry JA, Phan A, Davis RL. 2018. Dopamine Neurons Mediate Learning and Forgetting through Bidirectional Modulation of a Memory Trace. *Cell Rep* **25**:651–662.e5.

Bitterman ME, Menzel R, Fietz A, Schäfer S. 1983. Classical conditioning of proboscis extension in honeybees (Apis mellifera). *J Comp Psychol* **97**:107–119.

769 Borst A, Heisenberg M. 1982. Osmotropotaxis inDrosophila melanogaster. *Journal of*
770 *Comparative Physiology ? A*. doi:10.1007/bf00612013
771 Brembs B, Heisenberg M. 2001. Conditioning with compound stimuli in Drosophila
772 melanogaster in the flight simulator. *J Exp Biol* **204**:2849–2859.
773 Burke CJ, Huetteroth W, Owald D, Perisse E, Krashes MJ, Das G, Gohl D, Silies M,
774 Certel S, Waddell S. 2012. Layered reward signalling through octopamine and
775 dopamine in Drosophila. *Nature* **492**:433–437.
776 Campbell RAA, Honegger KS, Qin H, Li W, Demir E, Turner GC. 2013. Imaging a
777 population code for odor identity in the Drosophila mushroom body. *J Neurosci*
778 **33**:10568–10581.
779 Cohn R, Morantte I, Ruta V. 2015. Coordinated and Compartmentalized
780 Neuromodulation Shapes Sensory Processing in Drosophila. *Cell* **163**:1742–1755.
781 Dabney W, Kurth-Nelson Z, Uchida N, Starkweather CK, Hassabis D, Munos R,
782 Botvinick M. 2020. A distributional code for value in dopamine-based reinforcement
783 learning. *Nature* **577**:671–675.
784 Eckstein N, Bates AS, Du M, Hartenstein V, Jefferis GSX, Funke J. 2020.
785 Neurotransmitter Classification from Electron Microscopy Images at Synaptic Sites
786 in Drosophila. *bioRxiv*. doi:10.1101/2020.06.12.148775
787 Eschbach C, Fushiki A, Winding M, Schneider-Mizell CM, Shao M, Arruda R, Eichler K,
788 Valdes-Aleman J, Ohyama T, Thum AS, Gerber B, Fetter RD, Truman JW, Litwin-
789 Kumar A, Cardona A, Zlatic M. 2020. Recurrent architecture for adaptive regulation
790 of learning in the insect brain. *Nat Neurosci* **23**:544–555.
791 Felsenberg J, Barnstedt O, Cognigni P, Lin S, Waddell S. 2017. Re-evaluation of
792 learned information in Drosophila. *Nature* **544**:240–244.
793 Felsenberg J, Jacob PF, Walker T, Barnstedt O, Edmondson-Stait AJ, Pleijzier MW, Otto
794 N, Schlegel P, Sharifi N, Perisse E, Smith CS, Lauritzen JS, Costa M, Jefferis
795 GSXE, Bock DD, Waddell S. 2018. Integration of Parallel Opposing Memories
796 Underlies Memory Extinction. *Cell* **175**:709–722.e15.
797 Gewirtz JC, Davis M. 2000. Using pavlovian higher-order conditioning paradigms to
798 investigate the neural substrates of emotional learning and memory. *Learn Mem*
799 **7**:257–266.
800 Gewirtz JC, Davis M. 1997. Second-order fear conditioning prevented by blocking
801 NMDA receptors in amygdala. *Nature* **388**:471–474.
802 Gkanias E, McCurdy LY, Nitabach MN, Webb B. 2022. An incentive circuit for memory
803 dynamics in the mushroom body of. *Elife* **11**. doi:10.7554/eLife.75611
804 Handler A, Graham TGW, Cohn R, Morantte I, Siliciano AF, Zeng J, Li Y, Ruta V. 2019.
805 Distinct Dopamine Receptor Pathways Underlie the Temporal Sensitivity of
806 Associative Learning. *Cell* **178**:60–75.e19.
807 Hawkins RD, Greene W, Kandel ER. 1998. Classical conditioning, differential
808 conditioning, and second-order conditioning of the Aplysia gill-withdrawal reflex in a
809 simplified mantle organ preparation. *Behavioral Neuroscience*. doi:10.1037/0735-
810 7044.112.3.636
811 Helmstetter FJ, Fanselow MS. 1989. Differential second-order aversive conditioning
812 using contextual stimuli. *Animal Learning & Behavior*. doi:10.3758/bf03207636
813 Herendeen D, Chris Anderson D. 1968. Dual effects of a second-order conditioned
814 stimulus: Excitation and inhibition. *Psychonomic Science*. doi:10.3758/bf03342385
815 Hige T, Aso Y, Modi MN, Rubin GM, Turner GC. 2015. Heterosynaptic Plasticity
816 Underlies Aversive Olfactory Learning in Drosophila. *Neuron* **88**:985–998.
817 Holland PC. 1977. Conditioned stimulus as a determinant of the form of the Pavlovian
818 conditioned response. *J Exp Psychol Anim Behav Process* **3**:77–104.
819 Holland PC, Rescorla RA. 1975. Second-order conditioning with food unconditioned

stimulus. *J Comp Physiol Psychol* **88**:459–467.
Huetteroth W, Perisse E, Lin S, Klappenbach M, Burke C, Waddell S. 2015. Sweet taste and nutrient value subdivide rewarding dopaminergic neurons in Drosophila. *Curr Biol* **25**:751–758.
Ichinose T, Aso Y, Yamagata N, Abe A, Rubin GM, Tanimoto H. 2015. Reward signal in a recurrent circuit drives appetitive long-term memory formation. *Elife* **4**:e10719.
Jacob PF, Waddell S. 2020. Spaced Training Forms Complementary Long-Term Memories of Opposite Valence in Drosophila. *Neuron* **106**:977–991.e4.
Jenett A, Rubin GM, Ngo T-TB, Shepherd D, Murphy C, Dionne H, Pfeiffer BD, Cavallaro A, Hall D, Jeter J, Iyer N, Fetter D, Hausenfluck JH, Peng H, Trautman ET, Svirskas RR, Myers EW, Iwinski ZR, Aso Y, DePasquale GM, Enos A, Hulamm P, Lam SCB, Li H-H, Laverty TR, Long F, Qu L, Murphy SD, Rokicki K, Safford T, Shaw K, Simpson JH, Sowell A, Tae S, Yu Y, Zugates CT. 2012. A GAL4-driver line resource for Drosophila neurobiology. *Cell Rep* **2**:991–1001.
Jiang L, Litwin-Kumar A. n.d. Models of heterogeneous dopamine signaling in an insect learning and memory center. doi:10.1101/737064
Karuppudurai T, Lin T-Y, Ting C-Y, Pursley R, Melnattur KV, Diao F, White BH, Macpherson LJ, Gallio M, Pohida T, Lee C-H. 2014. A hard-wired glutamatergic circuit pools and relays UV signals to mediate spectral preference in Drosophila. *Neuron* **81**:603–615.
Kim HF, Ghazizadeh A, Hikosaka O. 2015. Dopamine Neurons Encoding Long-Term Memory of Object Value for Habitual Behavior. *Cell* **163**:1165–1175.
Kim HF, Ghazizadeh A, Hikosaka O. 2014. Separate groups of dopamine neurons innervate caudate head and tail encoding flexible and stable value memories. *Front Neuroanat* **8**:120.
Kim SD, Rivers S, Bevins RA, Ayres JJ. 1996. Conditioned stimulus determinants of conditioned response form in Pavlovian fear conditioning. *J Exp Psychol Anim Behav Process* **22**:87–104.
Kirkhart C, Scott K. 2015. Gustatory learning and processing in the Drosophila mushroom bodies. *J Neurosci* **35**:5950–5958.
Klapoetke NC, Murata Y, Kim SS, Pulver SR, Birdsey-Benson A, Cho YK, Morimoto TK, Chuong AS, Carpenter EJ, Tian Z, Wang J, Xie Y, Yan Z, Zhang Y, Chow BY, Surek B, Melkonian M, Jayaraman V, Constantine-Paton M, Wong GK-S, Boyden ES. 2014. Independent optical excitation of distinct neural populations. *Nat Methods* **11**:338–346.
König C, Khalili A, Niewalda T, Gao S, Gerber B. 2019. An optogenetic analogue of second-order reinforcement in Drosophila. *Biol Lett* **15**:20190084.
Krashes MJ, Waddell S. 2008. Rapid consolidation to a radish and protein synthesis-dependent long-term memory after single-session appetitive olfactory conditioning in Drosophila. *J Neurosci* **28**:3103–3113.
Lewis LPC, Siju KP, Aso Y, Friedrich AB, Bulteel AJB, Rubin GM, Grunwald Kadow IC. 2015. A Higher Brain Circuit for Immediate Integration of Conflicting Sensory Information in Drosophila. *Curr Biol* **25**:2203–2214.
Li F, Lindsey JW, Marin EC, Otto N, Dreher M, Dempsey G, Stark I, Bates AS, Pleijzier MW, Schlegel P, Nern A, Takemura S-Y, Eckstein N, Yang T, Francis A, Braun A, Parekh R, Costa M, Scheffer LK, Aso Y, Jefferis GS, Abbott LF, Litwin-Kumar A, Waddell S, Rubin GM. 2020. The connectome of the adult Drosophila mushroom body provides insights into function. *Elife* **9**. doi:10.7554/eLife.62576
Lin S, Owald D, Chandra V, Talbot C, Huetteroth W, Waddell S. 2014. Neural correlates of water reward in thirsty Drosophila. *Nat Neurosci* **17**:1536–1542.
Liu C, Plaçais P-Y, Yamagata N, Pfeiffer BD, Aso Y, Friedrich AB, Siwanowicz I, Rubin

GM, Preat T, Tanimoto H. 2012. A subset of dopamine neurons signals reward for odour memory in Drosophila. *Nature* **488**:512–516.
Liu WW, Wilson RI. 2013. Glutamate is an inhibitory neurotransmitter in the Drosophila olfactory system. *Proc Natl Acad Sci U S A* **110**:10294–10299.
Maes EJP, Sharpe MJ, Usypchuk AA, Lozzi M, Chang CY, Gardner MPH, Schoenbaum G, Iordanova MD. 2020. Causal evidence supporting the proposal that dopamine transients function as temporal difference prediction errors. *Nat Neurosci* **23**:176–178.
McCurdy LY, Sareen P, Davoudian PA, Nitabach MN. 2021. Dopaminergic mechanism underlying reward-encoding of punishment omission during reversal learning in Drosophila. *Nat Commun* **12**:1115.
Mizunami M, Unoki S, Mori Y, Hirashima D, Hatano A, Matsumoto Y. 2009. Roles of octopaminergic and dopaminergic neurons in appetitive and aversive memory recall in an insect. *BMC Biol* **7**:1–16.
Nern A, Pfeiffer BD, Rubin GM. 2015. Optimized tools for multicolor stochastic labeling reveal diverse stereotyped cell arrangements in the fly visual system. *Proc Natl Acad Sci U S A* **112**:E2967–76.
Owald D, Felsenberg J, Talbot CB, Das G, Perisse E, Huetteroth W, Waddell S. 2015. Activity of defined mushroom body output neurons underlies learned olfactory behavior in Drosophila. *Neuron* **86**:417–427.
Owald D, Waddell S. 2015. Olfactory learning skews mushroom body output pathways to steer behavioral choice in Drosophila. *Curr Opin Neurobiol* **35**:178–184.
Pai T-P, Chen C-C, Lin H-H, Chin A-L, Lai JS-Y, Lee P-T, Tully T, Chiang A-S. 2013. Drosophila ORB protein in two mushroom body output neurons is necessary for long-term memory formation. *Proc Natl Acad Sci U S A* **110**:7898–7903.
Pavlov IP. 1927. Lectures on conditioned reflexes: Twenty-five years of objective study of the higher nervous activity (behaviour) of animals. New York.
Perisse E, Owald D, Barnstedt O, Talbot CB, Huetteroth W, Waddell S. 2016. Aversive Learning and Appetitive Motivation Toggle Feed-Forward Inhibition in the Drosophila Mushroom Body. *Neuron* **90**:1086–1099.
Pettersson J. 1970. An Aphid Sex Attractant. *Insect Systematics & Evolution*. doi:10.1163/187631270x00357
Pfeiffer BD, Ngo T-TB, Hibbard KL, Murphy C, Jenett A, Truman JW, Rubin GM. 2010. Refinement of tools for targeted gene expression in Drosophila. *Genetics* **186**:735–755.
Plaçais P-Y, Trannoy S, Friedrich AB, Tanimoto H, Preat T. 2013. Two pairs of mushroom body efferent neurons are required for appetitive long-term memory retrieval in Drosophila. *Cell Rep* **5**:769–780.
Plaçais P-Y, Trannoy S, Isabel G, Aso Y, Siwanowicz I, Belliart-Guérin G, Vernier P, Birman S, Tanimoto H, Preat T. 2012. Slow oscillations in two pairs of dopaminergic neurons gate long-term memory formation in Drosophila. *Nat Neurosci* **15**:592–599.
Rescorla RA. 1980. Pavlovian Second-order Conditioning: Studies in Associative Learning. Psychology Press.
Rescorla RA, Furrow DR. 1977. Stimulus similarity as a determinant of Pavlovian conditioning. *J Exp Psychol Anim Behav Process* **3**:203–215.
Riemensperger T, Völler T, Stock P, Buchner E, Fiala A. 2005. Punishment prediction by dopaminergic neurons in Drosophila. *Curr Biol* **15**:1953–1960.
Rizley RC, Rescorla RA. 1972. Associations in second-order conditioning and sensory preconditioning. *J Comp Physiol Psychol* **81**:1–11.
Roeper J. 2013. Dissecting the diversity of midbrain dopamine neurons. *Trends Neurosci* **36**:336–342.

Scheffer LK, Xu CS, Januszewski M, Lu Z, Takemura S-Y, Hayworth KJ, Huang GB, Shinomiya K, Maitlin-Shepard J, Berg S, Clements J, Hubbard PM, Katz WT, Umayam L, Zhao T, Ackerman D, Blakely T, Bogovic J, Dolafi T, Kainmueller D, Kawase T, Khairy KA, Leavitt L, Li PH, Lindsey L, Neubarth N, Olbris DJ, Otsuna H, Trautman ET, Ito M, Bates AS, Goldammer J, Wolff T, Svirskas R, Schlegel P, Neace E, Knecht CJ, Alvarado CX, Bailey DA, Ballinger S, Borycz JA, Canino BS, Cheatham N, Cook M, Dreher M, Duclos O, Eubanks B, Fairbanks K, Finley S, Forknall N, Francis A, Hopkins GP, Joyce EM, Kim S, Kirk NA, Kovalyak J, Lauchie SA, Lohff A, Maldonado C, Manley EA, McLin S, Mooney C, Ndama M, Ogundeyi O, Okeoma N, Ordish C, Padilla N, Patrick CM, Paterson T, Phillips EE, Phillips EM, Rampally N, Ribeiro C, Robertson MK, Rymer JT, Ryan SM, Sammons M, Scott AK, Scott AL, Shinomiya A, Smith C, Smith K, Smith NL, Sobeski MA, Suleiman A, Swift J, Takemura S, Talebi I, Tarnogorska D, Tenshaw E, Tokhi T, Walsh JJ, Yang T, Horne JA, Li F, Parekh R, Rivlin PK, Jayaraman V, Costa M, Jefferis GS, Ito K, Saalfeld S, George R, Meinertzhagen IA, Rubin GM, Hess HF, Jain V, Plaza SM. 2020. A connectome and analysis of the adult central brain. *Elife* **9**. doi:10.7554/eLife.57443

Schultz W. 1998. Predictive Reward Signal of Dopamine Neurons. *Journal of Neurophysiology*. doi:10.1152/jn.1998.80.1.1

Séjourné J, Plaçais P-Y, Aso Y, Siwanowicz I, Trannoy S, Thoma V, Tedjakumala SR, Rubin GM, Tchénio P, Ito K, Isabel G, Tanimoto H, Preat T. 2011. Mushroom body efferent neurons responsible for aversive olfactory memory retrieval in Drosophila. *Nat Neurosci* **14**:903–910.

Siju KP, Štih V, Aimon S, Gjorgjieva J, Portugues R, Grunwald Kadow IC. 2020. Valence and State-Dependent Population Coding in Dopaminergic Neurons in the Fly Mushroom Body. *Curr Biol* **30**:2104–2115.e4.

Sisk CL. 1976. Second-order Conditioning of the Pigeon's Key Peck Using Stimuli from Two Modalities.

Stanhope KJ. 1992. The representation of the reinforcer and the force of the pigeon's keypeck in first- and second-order conditioning. *Q J Exp Psychol B* **44**:137–158.

Starkweather CK, Uchida N. 2021. Dopamine signals as temporal difference errors: recent advances. *Curr Opin Neurobiol* **67**:95–105.

Stout S, Escobar M, Miller RR. 2004. Trial number and compound stimuli temporal relationship as joint determinants of second-order conditioning and conditioned inhibition. *Learn Behav* **32**:230–239.

Sun F, Zhou J, Dai B, Qian T, Zeng J, Li X, Zhuo Y, Zhang Y, Wang Y, Qian C, Tan K, Feng J, Dong H, Lin D, Cui G, Li Y. 2020. Next-generation GRAB sensors for monitoring dopaminergic activity in vivo. *Nat Methods* **17**:1156–1166.

Tabone CJ, de Belle JS. 2011. Second-order conditioning in Drosophila. *Learn Mem* **18**:250–253.

Takeda K. 1961. Classical conditioned response in the honey bee. *J Insect Physiol* **6**:168–179.

Tanaka NK, Tanimoto H, Ito K. 2008. Neuronal assemblies of the Drosophila mushroom body. *J Comp Neurol* **508**:711–755.

Tanimoto H, Heisenberg M, Gerber B. 2004. Experimental psychology: event timing turns punishment to reward. *Nature* **430**:983.

Tempel BL, Bonini N, Dawson DR, Quinn WG. 1983. Reward learning in normal and mutant Drosophila. *Proc Natl Acad Sci U S A* **80**:1482–1486.

Tully T, Quinn WG. 1985. Classical conditioning and retention in normal and mutant Drosophila melanogaster. *J Comp Physiol A* **157**:263–277.

Ueoka Y, Hiroi M, Abe T, Tabata T. 2017. Suppression of a single pair of mushroom

body output neurons in Drosophila triggers aversive associations. *FEBS Open Bio*. doi:10.1002/2211-5463.12203
Vrontou E, Groschner LN, Szydlowski S, Brain R, Krebbers A, Miesenböck G. 2021. Response competition between neurons and antineurons in the mushroom body. *Curr Biol* **31**:4911–4922.e4.
Wan Y, Otsuna H, Chien C-B, Hansen C. 2012. FluoRender: An Application of 2D Image Space Methods for 3D and 4D Confocal Microscopy Data Visualization in Neurobiology Research. *IEEE Pac Vis Symp* 201–208.
Watabe-Uchida M, Uchida N. 2018. Multiple Dopamine Systems: Weal and Woe of Dopamine. *Cold Spring Harb Symp Quant Biol* **83**:83–95.
Worden BD, Papaj DR. 2005a. Flower choice copying in bumblebees. *Biol Lett* **1**:504–507.
Worden BD, Papaj DR. 2005b. Flower choice copying in bumblebees. *Biol Lett* **1**:504–507.
Yamagata N, Ichinose T, Aso Y, Plaçais P-Y, Friedrich AB, Sima RJ, Preat T, Rubin GM, Tanimoto H. 2015. Distinct dopamine neurons mediate reward signals for short- and long-term memories. *Proc Natl Acad Sci U S A* **112**:578–583.
Yin H, Barnet RC, Miller RR. 1994. Second-order conditioning and Pavlovian conditioned inhibition: operational similarities and differences. *J Exp Psychol Anim Behav Process* **20**:419–428.
Zhao X, Lenek D, Dag U, Dickson BJ, Keleman K. 2018. Persistent activity in a recurrent circuit underlies courtship memory in. *Elife* **7**. doi:10.7554/eLife.31425
Zheng Z, Lauritzen JS, Perlman E, Robinson CG, Nichols M, Milkie D, Torrens O, Price J, Fisher CB, Sharifi N, Calle-Schuler SA, Kmecova L, Ali IJ, Karsh B, Trautman ET, Bogovic JA, Hanslovsky P, Jefferis GSXE, Kazhdan M, Khairy K, Saalfeld S, Fetter RD, Bock DD. 2018. A Complete Electron Microscopy Volume of the Brain of Adult Drosophila melanogaster. *Cell* **174**:730–743.e22.
Zolin A, Cohn R, Pang R, Siliciano AF, Fairhall AL, Ruta V. 2021. Context-dependent representations of movement in Drosophila dopaminergic reinforcement pathways. *Nat Neurosci* **24**:1555–1566.

Figure legends

Figure 1. Appetitive olfactory second-order conditioning in Drosophila
(A) A simplified diagram of the mushroom body circuit. Identity of odors are encoded by patterns of activity in ~2,000 Kenyon cells. Contingent activity of Kenyon cells and dopamine release leads to plasticity of excitatory synapses from Kenyon cells to MB output neurons with compartment-specific dynamics.
(B) A diagram of the four-armed olfactory arena. Flies were confined in the 9 cm diameter circular area above the LED board. For odor-sugar conditioning, flies were first trained in a tube by pairing an odor with dried sugar paper, and then introduced to the olfactory arena. Performance index was calculated by counting the number of flies in each quadrant (see Methods).
(C) Dynamics of MCH preference after various 2 or 5 min of first-order conditioning with sugar. Flies were trained after 40-48 hours of starvation and memories were tested 20-24 hours later without feeding in between by examining preference to MCH over air for 12 times. Unpaired group received 5 min of sugar 2 min prior to 5 min exposure to MCH. Mean performance index of the first 5 tests after 5 min training was higher than that of 2 min. $p<0.01$; unpaired t-test; N=10-12.
(D) Second-order memory performance by wild type flies. n.s., not significant ($p=0.152$); ***, $p<0.0001$; Dunn's multiple comparison tests following Kruskal-Wallis test; N = 14–16. Means and SEMs are displayed with individual data points.
(E) The odor preference following the sensory preconditioning protocol, in which the order of the first and second-order conditioning was swapped. n.s., not significantly different from the chance level; Wilcocxon signed-rank test; N=12.
(F) Retention of second-order memory. After 24-hour, the second-order memory decayed to the chance level. ***, $p<0.001$; Wilcocxon signed-rank test or Mann-Whiteney test; N = 12.
(G) Odor preference between two S2 odors after the second-order or first-order conditioning was measured for six times by alternative position of two odorants with 2 min intervals. Memory persistency, a mean of PIs for 3rd-6th tests divided by PI of 1st test, was significantly smaller for second-order memory. **; $p<0.0022$; Mann-Whitney test; N=6. Means and SEMs are displayed with individual data points.

(H) Learning curves by first-order, second-order, or second-order without omission of optogenetic reward. Flies expressing CsChrimson in sugar sensory neurons with Gr64f-GAL4 were trained by pairing S2+ odor with activation of LED (First) or S1 odor that was previously paired with LED (Second). In the no omission protocol, sugar sensory neurons were activated immediately after S1 by repeating 1s red LED illumination with 1s intervals for three times. Preference between S2+ and S2- odors was tested after 1st, 3rd, 5th, 7th and 9th training sessions. After 9th training, memory by second-order protocol was lower than other protocols and its peak at 3rd training ($p<0.05$); Dunn's multiple comparison tests following Kruskal-Wallis test; N=8.
(I) Learning of S2 odors was compromised when S1 odor paired with Gr64f>CsChrimson precedes S2+ odor. *, $p<0.05$ by Dunn's tests following Kruskal-Wallis test; N=12.

Figure 1-soure data 1

Figure 1-figure supplement 1 Dynamics of odor preference
(A)Twelve repetition of odor preference of fed and 40-48 hour starved flies.
PIs represent results of reciprocal experiments. The half groups of flies went through the identical tests but with alternating positions of odors and air quadrants to cancel out potential positional preference for each rigs. The mean odor preferences during 12 tests were significantly different between fed and starved flies for MCH and EL. $p<0.01$; unpaired t-test; N=8. Means and SEM are shown.
(B) Delta between the first test and subsequent tests in fed (left) and 40-48 hour starved flies (right). Areas under curve for OCT was significantly higher than that for other odors in both fed and starve flies, whereases the area under the curve for MCH was lower than other odors only in starved flies. $p<0.01$; unpaired t-test; N=8.

Figure 1-figur supplement 1-soure data 1

Figure 2. Identification of the teacher compartment(s)
(A) Dynamics of S1 odor (MCH) preference after pairing 1 min of S1 odor with activation of different PAM cluster DANs for three times. Numbers of CsChrimson-mVenus in each driver per hemisphere and total number of corresponding DAN cell types in EM hemibrain data are indicated. At 3rd-7th tests, MCH preference of MB043C>CsChrimson flies was higher than all other genotypes. $p<0.05$; Dunn's multiple comparison tests following Kruskal-Wallis test; N=6.
(B) The second-order conditioning 2-min or 1 day after the first-order conditioning with optogenetic activation of various DAN types. Second-order memory was tested immediately after pairing S2+ odor with S1 odor (MCH) five times. n.s., not significant; *, $p=0.0330$; **, $p=0.0046$ ***, $p<0.001$; Dunn's multiple comparison tests following Kruskal-Wallis test; N=8-10.
(C) The second-order memory immediately after backward second-order conditioning. Flies expressing CsChrimon-mVenus by MB043C split-GAL4 were trained with identical protocol as in B, except that the onset of S1 odor was shifted to the 10 second before the onset of the first S2 odor. n.s., not significant from zero; Wilcocxon signed-rank test; N=6.
(D) Preference to the S1 odor (left) and second-order memory (right) by flies expressing TNT with empty, MB196B or MB043C split-GAL4. MB196B labels ~27 cells per hemisphere, including PAM-γ4, PAM-γ4<γ1γ2, γ5 and β′2a. *, $p=0.0126$; ***, $p<0.001$; Dunn's multiple comparison tests following Kruskal-Wallis test; N=8 for S1 preference; N=10-14 for second-order.

(F) Learning curves by first-order, second-order, or second-order without omission of optogenetic reward. Flies expressing CsChrimson with MB043C split-GAL4 were trained by pairing S2+ odor directly with optogenetic activation of DANs (First) or S1 odor that was previously paired with DAN activation (Second). In the no omission protocol, DANs were activated immediately after S1 by repeating 1s red LED illumination with 1s intervals for three times. Preference between S2+ and S2- odors was tested after 1st, 3rd, 5th, 7th and 9th training sessions. After 9th training, memory by second-order protocol was lower than other protocols and its peak at 5th training. **, $p<0.01$; Dunn's multiple comparison tests following Kruskal-Wallis test; N=8-10.
(G) The preference for the S1 odor (MCH) after the 9th session of second-order conditioning as in F. n.s., not significant; Mann-Whitney test; N=8.
(H) Comparison of memory decay after repetitive tests. Flies were trained five times with first or second-order conditioning protocol as in F but without tests. Immediately after the 5th training, preference between two S2 odors was measured repeatedly without training. At third test, second-order memory was significantly lower than first-order memory. **, $p=0.0036$; Dunn's multiple comparison tests following Kruskal-Wallis test; N=8.

Figure 2-source data 1

Figure 3. Second-order Conditioning Induces Cross-compartmental Plasticity.
(A) Experimental design and protocol. ChrimsonR-mVenus was selectively expressed in PAM-α1 using MB043-split-LexA (*58E02-ZpLexADBD in JK22C; 32D11-p65ADZp in JK73A*; see Figure 3-figure supplement 1 for expression pattern), and in vivo whole-cell recordings were made from MBON-γ5β′2a, which was labeled by mScarlet using a split-GAL4 driver *SS01308*. For the first-order conditioning, 1-min presentation of S1 (MCH) was paired with LED stimulation (1 ms, 2 Hz, 120 times), which caused odor-specific suppression of responses in MBON-α1 (Figure 3-figure supplement 2). After repeating first-order conditioning three times with 2-min intervals, second-order conditioning was performed by presenting S2+ (either PA or EL) for 20 s, and then S1 for 10 s with 5-s delay. S2− was presented alone 2 min later. Second-order conditioning was repeated five times, and the responses to S2 were recorded. In control experiments, first-order conditioning was performed in the same manner, but the presentation of S1 was omitted during second-order conditioning. Reciprocal experiments were performed by swapping S2+ and S2− in separate flies.
(B) Mean responses (± SEM in light colors) to S2+ and S2− in the first (black) and fifth trials (red) during second-order conditioning (n = 14, including reciprocal experiments). Horizontal gray bars indicate 20-s odor presentation period.
(C) Mean response magnitudes (± SEM) evoked by S2+ and S2−. The response magnitude was calculated by averaging the depolarization during the response window (0–20.6 s from odor onset). Each solid (PA used as S2+; n = 7) and dashed line (EL as S2+; n = 7) indicates data from a single fly. Responses to S2+ underwent depression after the first trial, while those to S2− did not change. Different letters indicate significant differences detected by Tukey's post hoc multiple comparisons test ($p < 0.05$) following repeated-measures two-way ANOVA ($p = 0.003$). There was no significant change in the peak amplitude ($p = 0.87$).
(D, E) Same as (B) and (C) except that the data are from control experiments (n = 4 each with PA or EL used as S2+, respectively). Neither responses to S2+ nor S2− changed ($p = 0.28$; repeated-measures two-way ANOVA). The peak response did not change either ($p = 0.22$).

Figure 3-figure supplement 1 Expression patterns of MB043-split-LexA, MB319C and SS67221-split-GAL4

(A) MB043-split-LexA drove expression ChrimsonR-mVenus in 4.7 PAM-α1 neurons on average: (4, 4, 5, 4, 5, 6) cells per hemisphere were observed in three brain samples.

(B-C) The expression pattern of MB043-split-LexA was unaffected in the presence of MB319C-split-GAL4. We observed a few additional mScarlet-positive cells in addition to the two MBON-α1, presumably because interference between the AD hemi-driver of the MB043-split-LexA and DBD hemi-driver of MB319C-split-GAL4. For electrophysiology, MBON-α1 was found based on their soma location, brightness of mScarelt signals and odor response.

(D-E) Expression patterns of MB043-split-LexA and SS67221-GAL4-split-GAL4. Additional cells expressed mScarlet in optic lobes, but MBON-γ5β′2a was unambiguously labeled by mScarlet in the central brain.

(F-G) Expression patterns of MB043-split-LexA and SS67221-GAL4-split-GAL4 did not interfere.

Figure 3-figure supplement 2 Optogenetic Conditioning in α1 Compartment Induces Depression in MBON-α1

(A) Experimental design and protocol. ChrimsonR-mVenus was selectively expressed in PAM-α1 using MB043-split-LexA, and in vivo whole-cell recordings were made from MBON-α1, which was labeled by mScarlet using a split-GAL4 driver MB319C. 1-min presentation of CS+ (OCT or MCH) was paired with LED stimulation (1 ms, 2 Hz, 120 times), followed by 1-min presentation of CS− alone. Reciprocal experiments were performed by swapping CS+ and CS− in a separate set of flies.

(B) Membrane voltage (upper panels) and spike data (lower panels) from a single representative fly, in which OCT was used as CS+. Gray bars indicate 1-s odor presentation.

(C) Time courses of instantaneous spike rate (mean ± SEM; n = 6 and 5 for each set of experiment).

(D) Summary data of mean odor-evoked spike counts (± SEM). Gray lines indicate data from individual neurons. After each pairing, responses to CS+ were suppressed, while those to CS− were either showed less suppression than CS+ or no change (repeated-measures two-way ANOVA followed by Tukey's post hoc multiple comparisons test; *$p < 0.05$, **$p < 0.005$, ***$p < 0.001$).

Figure 3-figure supplement 3. Response to current injection in MBON-γ5β′2a

Representative somatic voltage responses to current injection in MBON-γ5β′2a with (right) or without (left) TTX (1 mM). The current injection waveforms are shown in the inset in the middle. Depolarization typically increased the frequency of small, fast membrane potential fluctuations, which were partially suppressed by TTX. However, those events were not readily distinguishable from the putative synaptic potentials that were remaining in the presence of TTX. Therefore, it remains inconclusive whether MBON-γ5β′2a elicits action potentials.

Figure 4. SMP108 is a key interneuron between MBON-α1 and DANs

(A)The connections from MBON-α1 to PAM cluster DANs with two interneurons identified in the hemibrain EM data (Scheffer et al., 2020). The width of arrows indicate number of connections. The colors of circles and arrows indicate type of putative neurotransmitter. Single SMP353 and three SMP354s have similar morphology and

projection patterns and converge on to SMP108. Cholinergic interneurons SMP353/SMP354 and SMP108 are shown as filled orange circles and arrows. Other cholinergic connections are shown in transparent orange. See Supplementary File 1 for a full connectivity matrix and neurotransmitter predictions. See Figure 4-figure supplement 2 for the SMP108's connections with subtypes of DANs.
(B) Connections between the six neurons in the second layer in A and CRE011. SMP108 outputs to all three other putative cholinergic interneurons. LHPV10d1 is the top target of SMP108. SMP553 send its first and second strongest outputs to SMP108 and SMP177.
(C) Total number of connections to reward DANs (PAM01, 02, 04, 06, 07, 08, 10, 11,15) which can induce appetitive memory with optogenetic activation, plotted against number of inputs from MBON-γ5β′2a. Each circle represents one of 396 interneuron cell types that have at least 100 total connections with MBONs and DANs. Similar to SMP108, CRE011 is an outlier cell type in terms of the high number of direct inputs from MBON-γ5β′2a and outputs to reward DANs. See Figure 4-figure supplement 3 for other kinds of connections between these interneurons and DANs/MBONs.
(D) A projection of a reconstructed SMP108 neuron in the hemibrain EM images aligned to a standard brain with outline of the brain and the MB lobes.
(E) Confocal microscope images of SS67221 split-GAL4 driver with membrane-targeted reporter myr-smFLAG and presynaptic reporter Syt-smHA. Inset shows anti-ChAT immunoreactivity of SMP108's axon terminals. (F) Morphology of individual SMP108 visualized by multi-color flip out of SS67221 split-GAL4.

Figure 4-figure supplement 1 Connections of MBON-α1 and SMP108
(A) Numbers of direct MBON-to-DANs synaptic connections. White boxes indicate within-a-compartment connection such as connection from MBON-α1 to PAM-α1.
(B) Total number of outputs to reward DANs (i.e. PAM01, 02, 04, 06, 07, 08, 10, 11,15) which can induce appetitive memory upon optogenetic activation, plotted against total number of connection from MBON-α1 for 396 cell types that have at least 100 total connections with MBONs and DANs. Colors indicate predicted neurotransmitters. One of outstanding cell type, LHAD1b5, cannot mediate cross-compartmental pathways because it is exclusively connected with PAM-α1 but not other reward DANs. Another outstanding cell type LHAD1b2_d is a part of two-hop pathways from MBON-α1 to PAM-α1 (Figure 3A)
(C) Total number of outputs to reward DANs plotted against total number of outputs to punishment DANs (i.e. PPL101, 103, 105, 106 and PAM12).

Figure 4-figure supplement 2 Connections from SMP108 to DAN subtypes
The number in the top row is the total number of connections from the SMP108 to subtypes of DANs that were defined by their projection and connectivity patterns (Li et al., 2020). The number of cells per subtype and number of connections per cell are shown in the middle and bottom row, respectively.

Figure 4-figure supplement 3 Connections of interneurons with DANs and MBONs
Scatter plots display designated pairs of connections for 396 cell types that have at least 100 total connections with MBONs and DANs in EM hemibrain data. Colors indicate predicted neurotransmitters. Names of outlier cell types are labeled. See Supplementary Table 1 for full data. Note that SMP354 and other cholinergic interneurons in 2-hop

pathway (Figure 4A), SMP177, LHPV5e1, LHAD1b2_d, LHPV10d1 showed a shared property of receiving converging inputs from glutamatergic MBONs and cholinergic MBONs, whose activity represent appetitive or aversive memories, respectively. In addition to input from MBON-α1, SMP354 receive converging inputs from MBON-α3, a compartment of long-term aversive memory.

Figure 5. SMP108 acquires enhanced responses to reward-predicting odors
(A) Experimental design and protocol. ChrimsonR-mVenus was expressed in PAM-cluster DANs, which include PAM-α1, using R58E02-LexA. In vivo whole-cell recordings were made from SMP108, which was labeled by GFP using a split-GAL4 driver SS45234. In the first pairing (Pairing 1), 1-min presentation of OCT was paired with LED stimulation (1 ms, 2 Hz, 120 times), followed by 1-min presentation of MCH alone. Odors were flipped in the second round of pairing (Pairing 2). Responses to each odor (1-s presentation) were measured before (Pre) and after pairing 1 (Post 1), and after pairing 2 (Post 2).
(B) Membrane voltage (upper panels) and spike data (lower panels) from a single representative neuron. Gray bars indicate 1-s odor presentation.
(C) Time courses of instantaneous spike rate (mean ± SEM; n = 6).
(D) Summary data of mean odor-evoked spike counts (± SEM). Gray lines indicate data from individual neurons. After each pairing, responses to paired odors were potentiated, while those to unpaired odors tended to decrease. Repeated-measures two-way ANOVA ($p = 0.0001$) followed by Tukey's post hoc multiple comparisons test. *$p < 0.05$.

Figure 6. SMP108 promotes dopamine release in multiple compartments
(A) Representative images of Chrimson88-tdTtomato expression patterns (left) and maximum intensity projections of DA2m dF/F in the MB lobes (right). Release of dopamine upon activation of DANs or SMP108 pathways, measured with dopamine sensor DA2m expressed in Kenyon cells. *10XUAS-Syn21-Chrimson88-tdTtomato-3.1 in attP18* was driven with designated split-GAL4 driver lines. Fluorescence of DA2m in response to one second of 660nm LED light was measured in dissected brains with two-photon imaging of volume containing MB lobes (see Methods).
(B) Mean DA2m dF/F in ROIs defined for each MB compartment. SEMs are shown as shading, although they are often within width of lines representing means. N=8-12.
See Figure 6-figure supplement 1 for quantification and the data with direct simulation of DANs.

Figure 6-figure supplement 1. Patterns of dopamine release by different driver lines
Representative images of neurons expressing Chrimson88-tdTtomato by designated driver lines (left) and maximum intensity projection of DA2m dF/F in the MB lobes (right).
(A) Representative images of Chrimson88-tdTtomato expression patterns (left) and max intensity projections of DA2m dF/F in the MB lobes (right) as in Figure 6A.
(B) Mean DA2m dF/F in ROIs defined for each MB compartment. N=8-12.
(C) Area under the curve during the 10s period after activation.

Figure 6-figure supplement 1-source data 1

Figure 7. SMP108 is required for second-order memory
(A) Second-order memory immediately after 5 training sessions as in Figure 1D following 5min first order conditioning a day before. Blocking SMP108 by expressing TNT with SS67221 or SS45234 impaired the second-order memory compared to genetic controls. N=10-12.
(B) Preference to the S1 (MCH) odor over the air one day after pairing with sugar for 5min. N=8-10.
(C) First-order memory immediately after pairing S2+ odor with sugar for 2-min. N=8. *, $p<0.05$; **, $p<0.01$; Dunn's multiple comparison tests following Kruskal-Wallis test

Figure 7-source data 1

Figure 7-figure supplement 1 SMP108 can drive upwind steering but dispensable for the conditioned responses
(A) Diagram of the circular arena (top). Airflow was constantly set at 400mL/min throughout the experiments, and 10s of 627nm LED stimulations was applied for six times with 2min intervals. Six trial averages of upwind displacement from the onset of LED (middle) and cosine of angle to upwind direction (bottom) are shown for flies expressing CsChrimson SS67221 (SMP108) or empty-split-GAL4. SS67221>CsChrimson flies showed enhanced upwind displacement ($p<0.05$) and orientation toward upwind during LED ON period ($p<0.01$); See the method for the calculation of upwind displacement. N=12.
(B) Groups of flies were trained by pairing either PA or EL with sugar for 2-min, and their response to airflow in the presence of odors were examined 20-24 hours later. Flies showed enhanced upwind displacement and orientation to upwind in the presence of reward-predicting odor. Upwind steering of flies with blocked SMP108 (SS67221/UAS-TNT) was indistinguishable with control genotypes. N=15-16

Figure 7-figure supplement 1-source data 1

Figure 8. SMP108 pathway induces transient memory
(A) Teacher-student compartments model of second-order conditioning hypothesizes that "teacher" compartment with slow learning rate and persistent memory instructs other compartments with faster learning rate and transient memory dynamics via SMP353/SMP354 and SMP108.
(B) Dynamics of memory with optogenetic activation of SMP108 (SS67221), SMP353/354 (SS33917) or various types of DANs. See texts and methods for explanation of the protocol, and Figure 8-figure supplement 1 for specificity of expression pattern in the central brain and the ventral nerve cord. Means and SEM are displayed. N=8-14.
(C) Learning rate defined as a (PI after first 10s training)/(peak PI during the first 5 training trials) for each driver line.
(D) Persistency during training defined as (PI after 5th training)/(peak PI during the first 5 training trials).
(E) Persistency of memory defined as (mean of PIs during 12 tests after first training trials)/(peak PI during the first 5x training trials).

(F) Resistance to DAN activation defined as (mean of last three tests following activation LED without odors)/(PI after 5th conditioning in re-reversal phase), which measures both transiency during training and extinction during 12 tests.
$p<0.05$; **, $p<0.01$; ***, $p<0.01$; Dunn's multiple comparison tests following Kruskal-Wallis test; N=8-14.
(G) The log-probability ratio of choosing the S2+ against S2- for SS67221 (SMP108) data were fitted best with weights of (0.57, 0.46,0.157,0,0,0) for data of DAN driver lines (MB032B, MB213B, MB312C, MB043C, MB109B and MB315C).

Figure 8-source data 1

Figure 8-figure supplement 1. Expression patterns of drivers
(A-H) Projection of confocal microscopy stacks for expression patterns of CsChrimson-mVenus driven by designated split-GAL4 driver lines in brains and ventral nerve cords. Confocal stacks are available at https://splitgal4.janelia.org

1

Key Resources Table				
Reagent type (species) or resource	**Designation**	**Source or reference**	**Identifiers**	**Additional information**
strain, strain background (Drosophila melanogaster)	Canton S	Martin Heisenberg	N.A.	
strain, strain background (Drosophila melanogaster)	*20xUAS-CsChrimson-mVenus attP18*	Klapoetke et al., 2014; PMID: 24509633	N.A.	
strain, strain background (Drosophila melanogaster)	*10XUAS-Chrimson88-tdTomato attP1*	Klapoetke et al., 2014; PMID: 24509633	N.A.	
strain, strain background (Drosophila melanogaster)	13XLexAop2-IVS-ChrimsonR-mVenus-p10 attP18	Vivek Jayaraman	N.A.	
strain, strain background (Drosophila melanogaster)	20XUAS-syn21-mScarlet-opt-p10 su(Hw)attp8	Glenn Turner	N.A.	
strain, strain background (Drosophila melanogaster)	*pJFRC200-10xUAS-IVS-myr::smGFP-HA in attP18*	Nern et al.,2015; PMID: 25964354	N.A.	
strain, strain background (Drosophila melanogaster)	*pJFRC225-5xUAS-IVS-myr::smGFP-FLAG in VK00005*	Nern et al.,2015; PMID: 25964354	N.A.	

strain, strain background (Drosophila melanogaster)	*pBPhsFlp2::PEST in attP3*	Nern et al.,2015; PMID: 25964354	N.A.	
strain, strain background (Drosophila melanogaster)	*pJFRC201-10XUAS-FRT>STOP>FRT-myr::smGFP-HA in VK0005*	Nern et al.,2015; PMID: 25964354	N.A.	
strain, strain background (Drosophila melanogaster)	*pJFRC240-10XUAS-FRT>STOP>FRT-myr::smGFP-V5-THS-10XUAS-FRT>STOP>FRT-myr::smGFP-FLAG_in_su(Hw)attP1*	Nern et al.,2015; PMID: 25964354	N.A.	
strain, strain background (Drosophila melanogaster)	*LexAop2-DA2m VK00005*	Sun et al., 2020; PMID: 33087905	N.A.	
strain, strain background (Drosophila melanogaster)	MB043-split-LexA	This paper	N.A.	Available from Aso lab
strain, strain background (Drosophila melanogaster)	*empty-split-GAL4 (p65ADZp attP40, ZpGAL4DBD attP2)*	Seeds et al., 2014; PMID: 25139955	N.A.	
strain, strain background (Drosophila melanogaster)	MB032B split-GAL4	Aso et al., 2014a; PMID: 25535793	N.A.	

strain, strain background (Drosophila melanogaster)	MB043C split-GAL4	Aso et al., 2014a; PMID: 25535793	N.A.	
strain, strain background (Drosophila melanogaster)	MB109B split-GAL4	Aso et al., 2014a; PMID: 25535793	N.A.	
strain, strain background (Drosophila melanogaster)	MB213B split-GAL4	Aso et al., 2014a; PMID: 25535793	N.A.	
strain, strain background (Drosophila melanogaster)	MB315C split-GAL4	Aso et al., 2014a; PMID: 25535793	N.A.	
strain, strain background (Drosophila melanogaster)	SS33917 split-GAL4	This paper	N.A.	Available from Aso lab
strain, strain background (Drosophila melanogaster)	SS45234 split-GAL4	This paper	N.A.	Available from Aso lab
strain, strain background (Drosophila melanogaster)	SS67221 split-GAL4	This paper	N.A.	Available from Aso lab
strain, strain background (Drosophila melanogaster)	UAS-TeNT	Keller et al., 2002: PMID: 11810637	N.A.	
antibody	anti-GFP (rabbit polyclonal)	Invitrogen	A11122 RRID:AB_221569	1:1000

antibody	anti-Brp (mouse monoclonal)	*Developmental Studies Hybridoma Bank*	nc82 RRID:AB_2341866	1:30
antibody	anti-ChAT (mouse monoclonal)	*Developmental Studies Hybridoma Bank*	ChAT4B1 RRID:AB_528122	1:50
antibody	anti-HA-Tag (mouse monoclonal)	Cell Signaling Technology	C29F4; #3724 RRID:AB_10693385	1:300
antibody	anti-FLAG (rat monoclonal	Novus Biologicals	NBP1-06712 RRID:AB_1625981	1:200
antibody	anti-V5-TAG Dylight-549 (mouse monoclonal)	Bio-Rad	MCA2894D549GA RRID:AB_10845946	1:500
antibody	anti-mous IgG(H&L) AlexaFluor-568 (goat polyclonal)	Invitrogen	A11031 RRID:AB_144696	1:400
antibody	anti-rabbit IgG(H&L) AlexaFluor-488 (goat polyclonal)	Invitrogen	A11034 RRID:AB_2576217	1:800
antibody	anti-mouse IgG(H&L) AlexaFluor-488 conjugated (donkey polyclonal)	Jackson Immuno Research Labs	715-545-151 RRID:AB_2341099	1:400
antibody	anti-rabbit IgG(H&L) AlexaFluor-594 (donkey polyclonal)	Jackson Immuno Research Labs	711-585-152 RRID:AB_2340621	1:500

antibody	anti-rat IgG(H&L) AlexaFluor-647 (donkey polyclonal)	Jackson Immuno Research Labs	712-605-153 RRID:AB_2340694	1:300
antibody	anti-Mouse IgG (H&L) ATTO 647N (goat polyclonal)	ROCKLAND	610-156-121 RRID:AB_10894200	1:100
antibody	anti-rabbit IgG (H+L) Alexa Fluor 568 (goat polyclonal)	Invitrogen	A-11036 RRID:AB_10563566	1:1000
chemical compound, drug	3-Octanol	Sigma-Aldrich	218405	
chemical compound, drug	4-Methylcyclohexanol	VWR	AAA16734-AD	
chemical compound, drug	Pentyl acetate	Sigma-Aldrich	109584	
chemical compound, drug	Ethyl lactate	Sigma-Aldrich	W244015	
chemical compound, drug	Paraffin oil	Sigma-Aldrich	18512	
software, algorithm	ImageJ and Fiji	NIH Schneider et al., 2012	https://imagej.nih.gov/ij/ http://fiji.sc/	
software, algorithm	MATLAB	MathWorks	https://www.mathworks.com/	

software, algorithm	Adobe Illustrator CC	Adobe Systems	https://www.adobe.com/products/illustrator.html	
software, algorithm	GraphPad Prism 9	GraphPad Software	https://www.graphpad.com/scientific-software/prism/	
software, algorithm	Python	Python Software Foundation	https://www.python.org/	
software, algorithm	neuPrint	HHMI Janelia	https://doi.org/10.25378/janelia.12818645.v1	
software, algorithm	Cytoscape	(Shannon et al., 2003)	https://cytoscape.org/	
software, algorithm	NeuTu	Zhao et al., 2018	https://github.com/janelia-flyem/NeuTu	
software, algorithm	ScanImage	Vidrio Technologies	https://vidriotechnologies.com/	
software, algorithm	VVDveiwer	HHMI Janelia	https://github.com/takashi310/VVD_Viewer	
other	Grade 3MM Chr Blotting Paper	Whatmann	3030-335	Used in glass vials with paraffin-oil diluted odours
other	mass flow controller	Alicat	MCW-200SCCM-D	Mass flow controller used for the olfactory arena

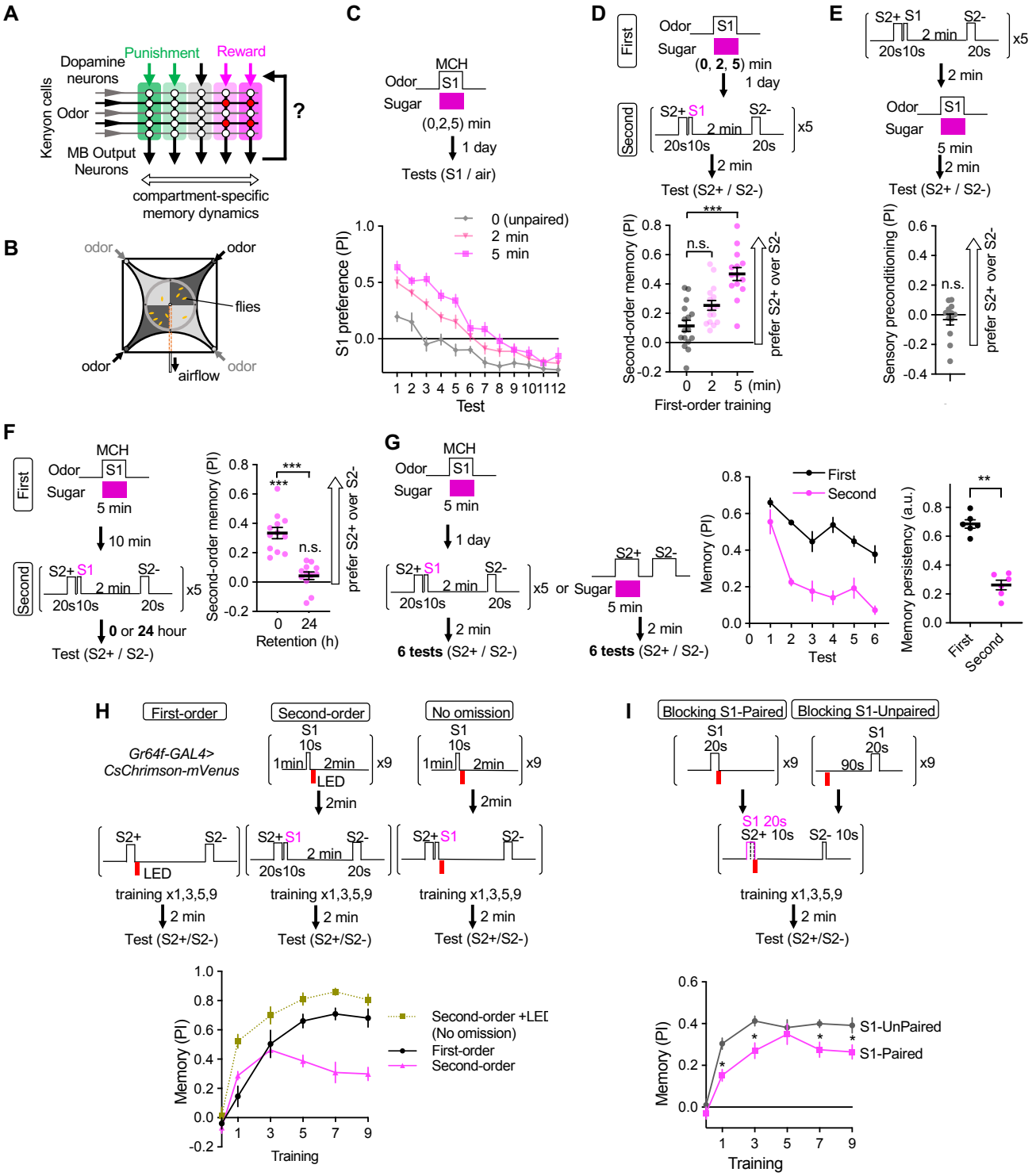
A
Dopamine neurons
Punishment
Reward
Kenyon cells
Odor
MB Output Neurons
?
compartment-specific memory dynamics
B
odor
odor
flies
odor
odor
airflow
C
MCH
Odor
S1
Sugar
(0,2,5) min
1 day
Tests (S1 / air)
0 (unpaired)
2 min
5 min
S1 preference (PI)
Test
D
First
Odor
S1
Sugar
(0, 2, 5) min
1 day
Second
S2+ S1
2 min
S2-
20s10s
20s
x5
2 min
Test (S2+ / S2-)
***
n.s.
Second-order memory (PI)
prefer S2+ over S2-
0 2 5 (min)
First-order training
E
S2+ S1
2 min
S2-
20s10s
20s
x5
2 min
Odor
S1
Sugar
5 min
2 min
Test (S2+ / S2-)
n.s.
Sensory preconditioning (PI)
prefer S2+ over S2-
F
First
MCH
Odor
S1
Sugar
5 min
10 min
Second
S2+ S1
2 min
S2-
20s10s
20s
x5
0 or 24 hour
Test (S2+ / S2-)
***
***
n.s.
Second-order memory (PI)
prefer S2+ over S2-
0 24
Retention (h)
G
MCH
Odor
S1
Sugar
5 min
1 day
S2+ S1
2 min
S2-
20s10s
20s
x5
2 min
6 tests (S2+ / S2-)
or Sugar
5 min
2 min
6 tests (S2+ / S2-)
First
Second
Memory (PI)
Test
**
Memory persistency (a.u.)
First
Second
H
First-order
Second-order
No omission
Gr64f-GAL4>
CsChrimson-mVenus
S1
10s
1min
2min
LED
x9
2min
S2+
S2-
LED
S2+ S1
2 min
S2-
20s10s
20s
training x1,3,5,9
2 min
Test (S2+/S2-)
Memory (PI)
Training
Second-order +LED
(No omission)
First-order
Second-order
I
Blocking S1-Paired
Blocking S1-Unpaired
S1
20s
x9
90s
S1 20s
S2+ 10s
S2- 10s
training x1,3,5,9
2 min
Test (S2+/S2-)
Memory (PI)
Training
S1-UnPaired
S1-Paired

Figure 1

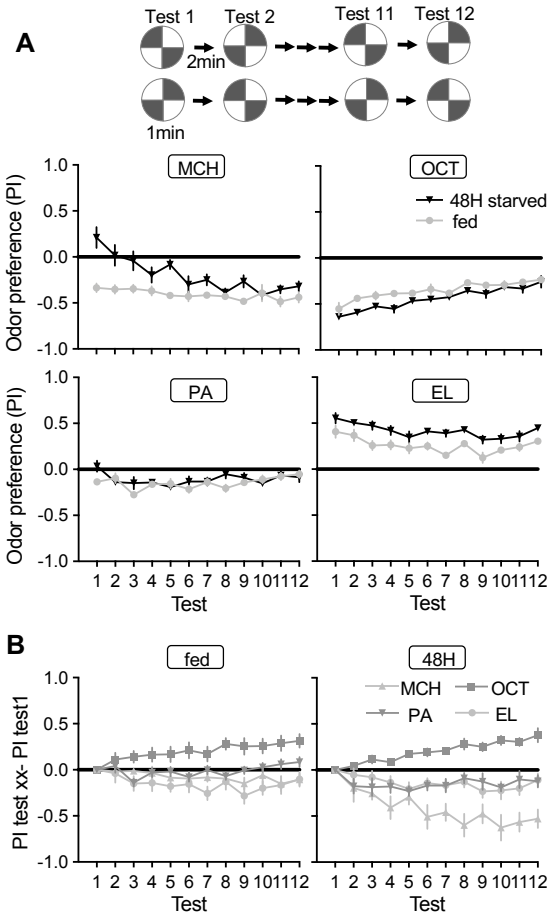

Figure 1-figure supplement 1

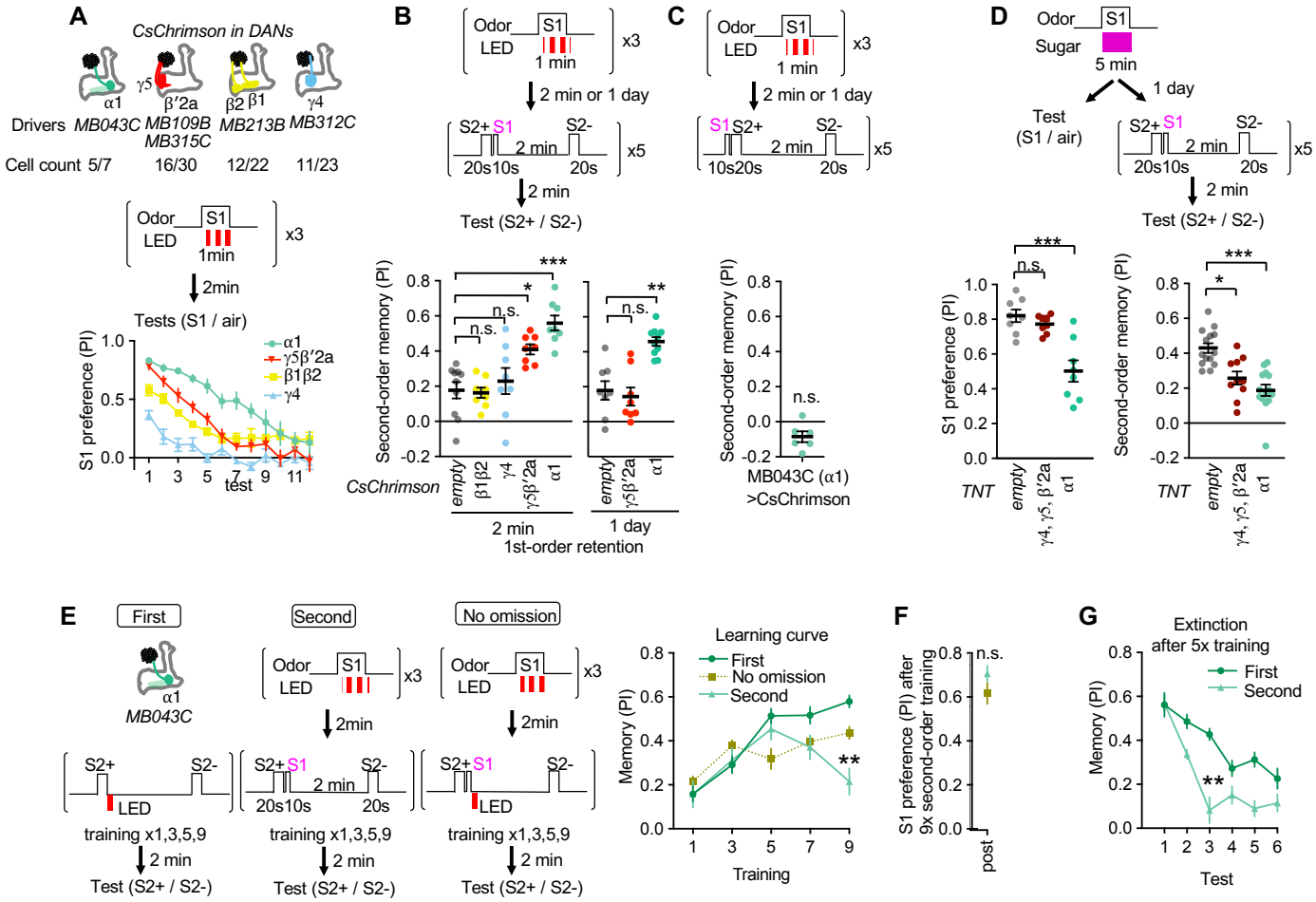
A
CsChrimson in DANs
α1
γ5 β′2a
β2 β1
γ4
Drivers MB043C MB109B MB315C MB213B MB312C
Cell count 5/7 16/30 12/22 11/23
Odor LED S1 1min x3
2min
Tests (S1 / air)
S1 preference (PI)
α1
γ5β′2a
β1β2
γ4
test
B
Odor LED S1 1 min x3
2 min or 1 day
S2+ S1 2 min S2- 20s 10s 20s x5
2 min
Test (S2+ / S2-)
Second-order memory (PI)
CsChrimson
empty β1β2 γ4 γ5β′2a α1
2 min
1 day
1st-order retention
C
Odor LED S1 1 min x3
2 min or 1 day
S1 S2+ 2 min S2- 10s 20s 20s x5
Second-order memory (PI)
MB043C (α1) >CsChrimson
D
Odor S1
Sugar 5 min
1 day
Test (S1 / air)
S2+ S1 2 min S2- 20s 10s 20s x5
2 min
Test (S2+ / S2-)
S1 preference (PI)
Second-order memory (PI)
TNT
empty γ4, γ5, β′2a α1
E
First
Second
No omission
α1
MB043C
Odor LED S1 x3
2min
S2+ S2- LED
S2+ S1 2 min S2- 20s 10s 20s
training x1,3,5,9
2 min
Test (S2+ / S2-)
Learning curve
First
No omission
Second
Memory (PI)
Training
F
S1 preference (PI) after 9x second-order training
post
G
Extinction after 5x training
First
Second
Memory (PI)
Test

Figure 2

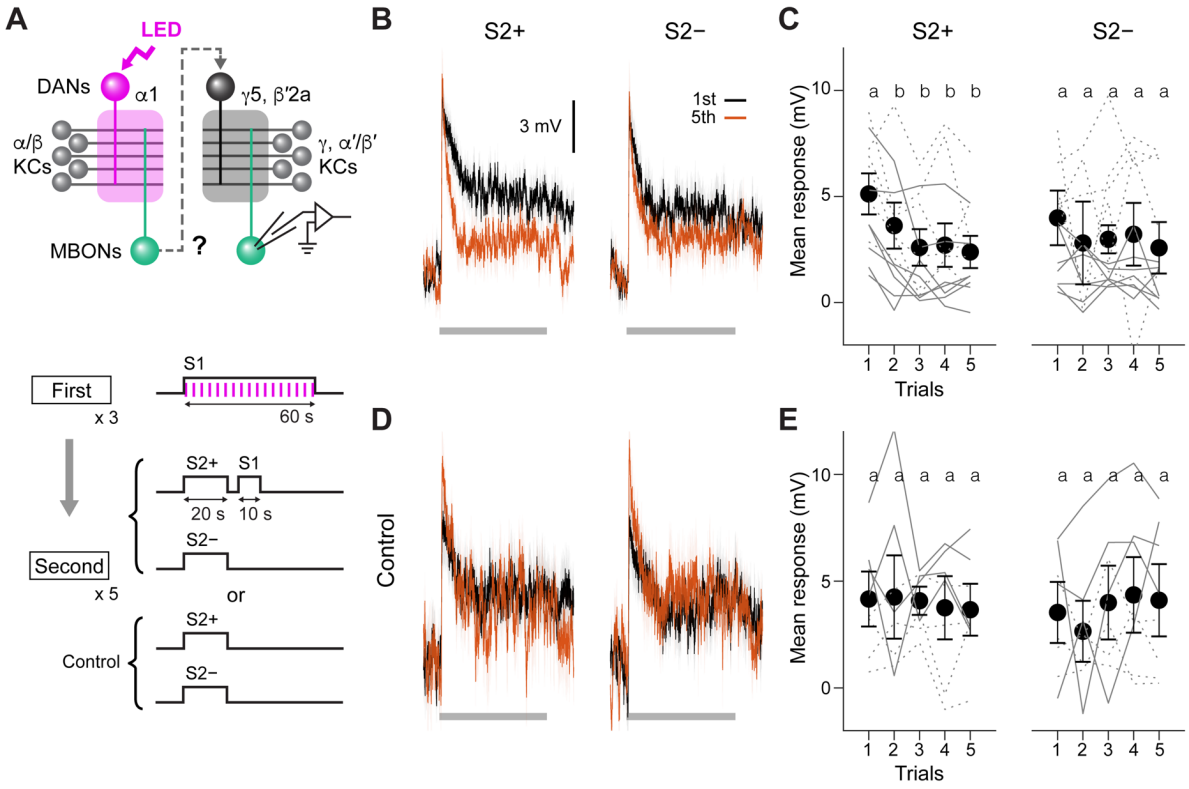
A
LED
DANs
α1
γ5, β′2a
α/β
KCs
γ, α′/β′
KCs
MBONs
?
First
x 3
S1
60 s
S2+
S1
20 s
10 s
S2−
Second
x 5
or
Control
S2+
S2−
B
S2+
S2−
3 mV
1st
5th
Control
C
S2+
S2−
Mean response (mV)
10
5
0
a b b b b
a a a a a
1 2 3 4 5
Trials
D
E
Mean response (mV)
a a a a a
a a a a a
Trials

Figure 3

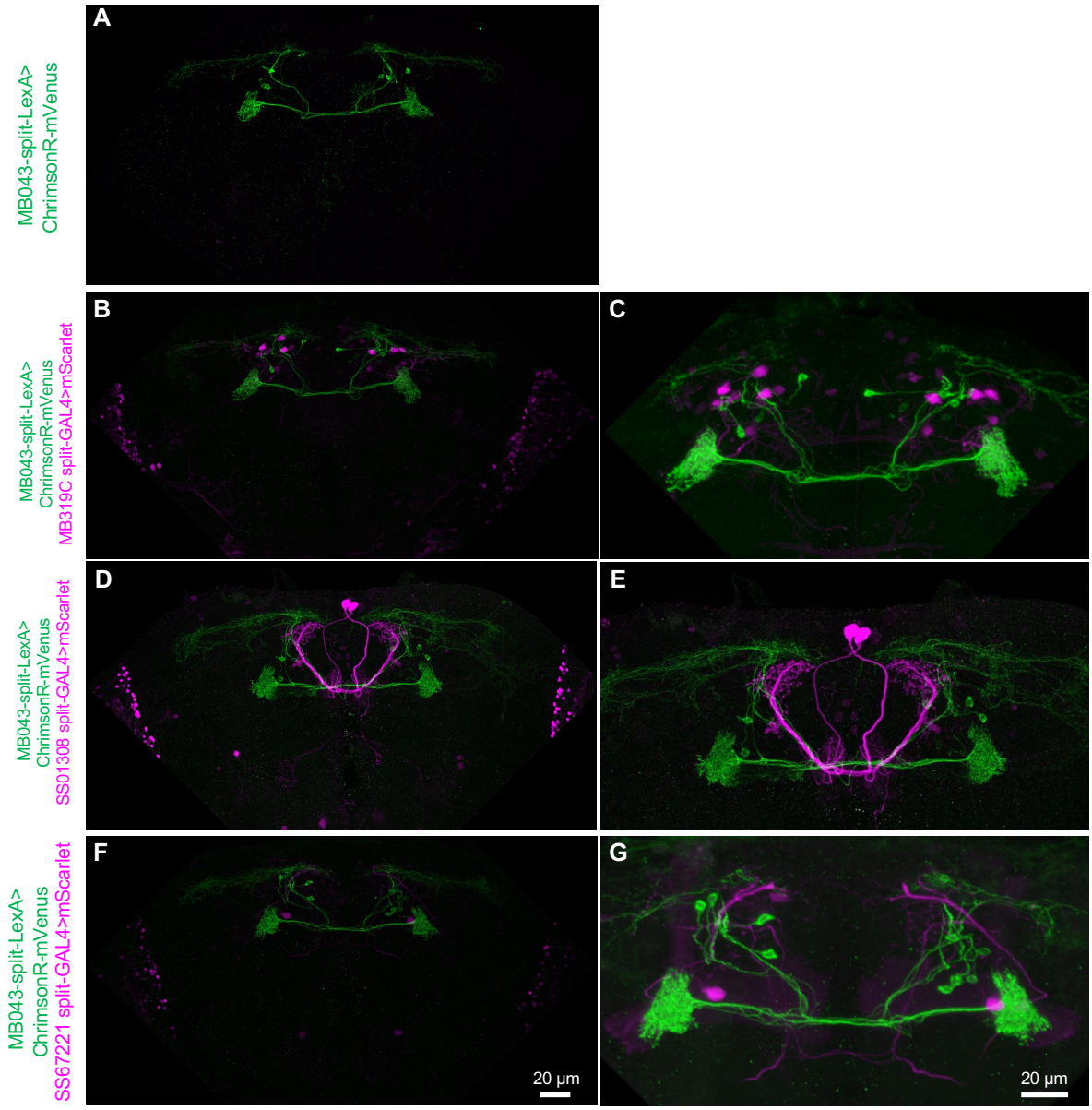

Figure 3-figure supplement 1

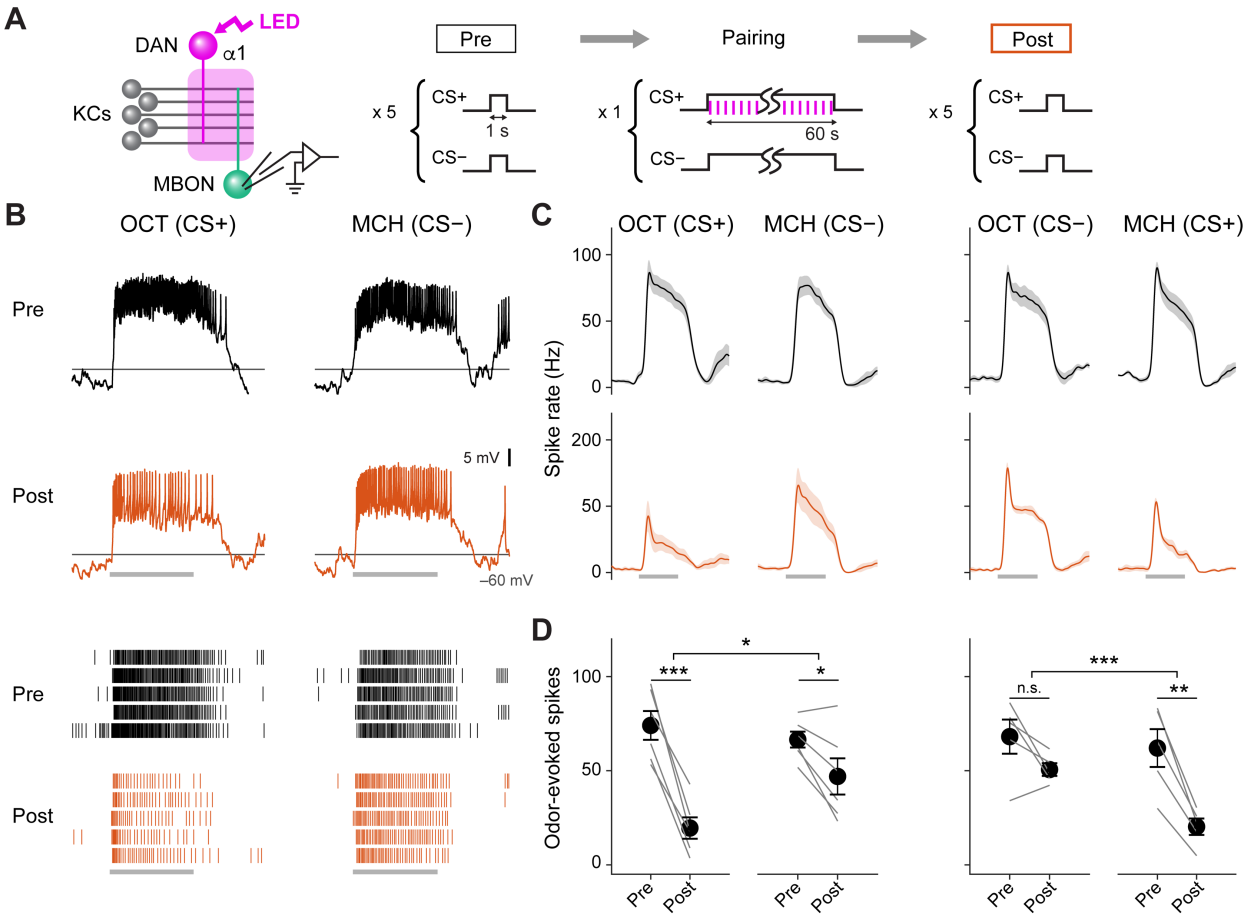

Figure 3-figure supplement 2

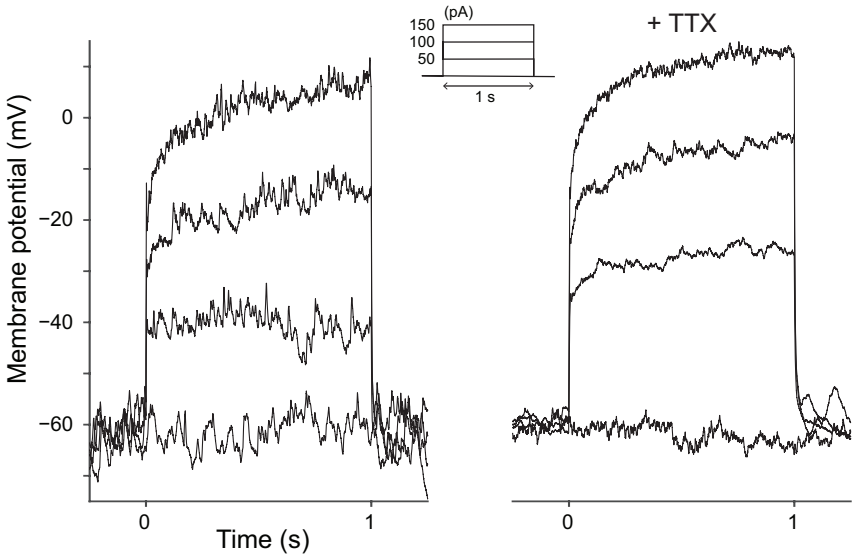

Figure 3-figure supplement 3

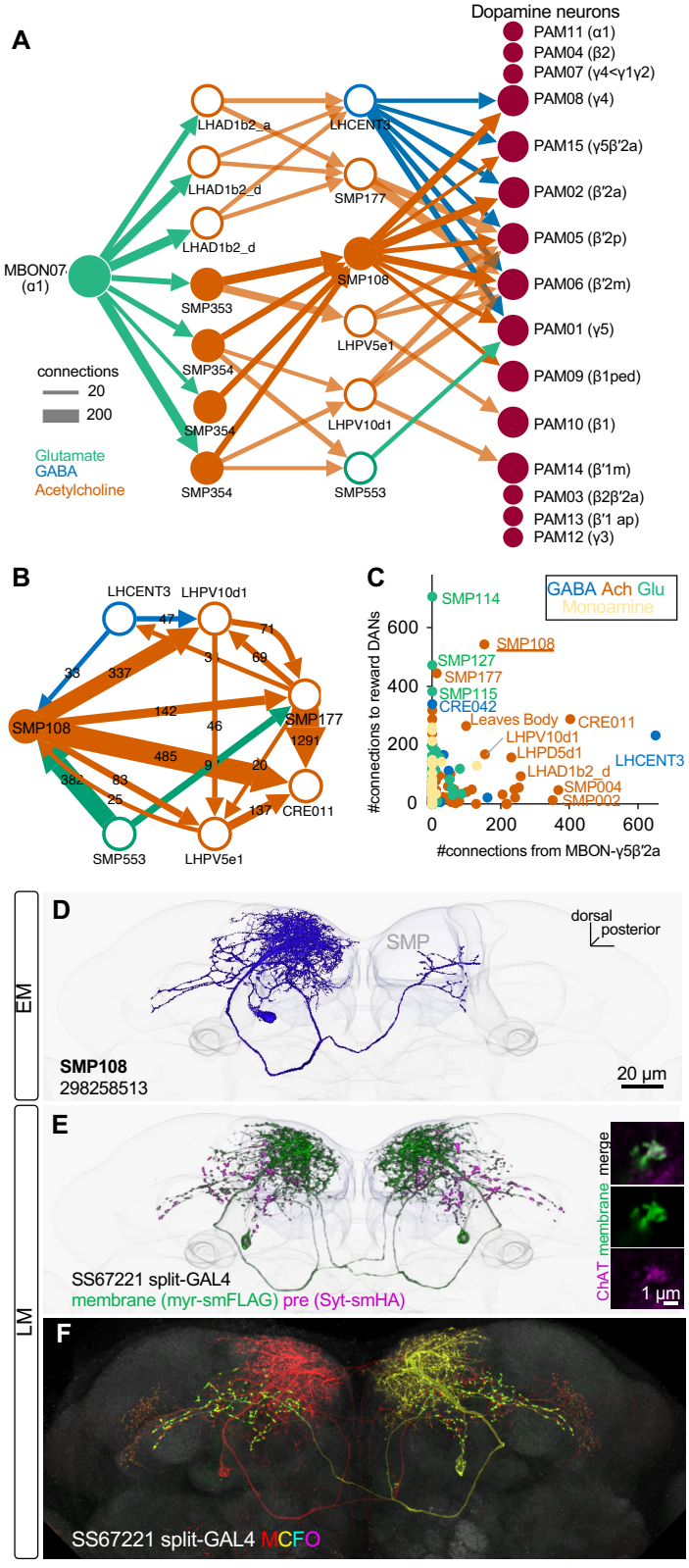
A
Dopamine neurons
PAM11 (α1)
PAM04 (β2)
PAM07 (γ4<γ1γ2)
PAM08 (γ4)
PAM15 (γ5β'2a)
PAM02 (β'2a)
PAM05 (β'2p)
PAM06 (β'2m)
PAM01 (γ5)
PAM09 (β1ped)
PAM10 (β1)
PAM14 (β'1m)
PAM03 (β2β'2a)
PAM13 (β'1 ap)
PAM12 (γ3)
LHAD1b2_a
LHAD1b2_d
LHAD1b2_d
MBON07
(α1)
SMP353
SMP354
SMP354
SMP354
LHCENT3
SMP177
SMP108
LHPV5e1
LHPV10d1
SMP553
connections
20
200
Glutamate
GABA
Acetylcholine
B
LHCENT3
LHPV10d1
47
71
3
69
38
337
142
46
SMP108
SMP177
1291
485
9
20
83
25
137
CRE011
SMP553
LHPV5e1
C
GABA Ach Glu
Monoamine
SMP114
SMP108
SMP127
SMP177
SMP115
CRE042
Leaves Body
CRE011
LHPV10d1
LHPD5d1
LHCENT3
LHAD1b2_d
SMP004
SMP002
#connections to reward DANs
0
200
400
600
#connections from MBON-γ5β'2a
D
EM
dorsal
posterior
SMP
SMP108
298258513
20 µm
E
LM
SS67221 split-GAL4
membrane (myr-smFLAG) pre (Syt-smHA)
merge
membrane
ChAT
1 µm
F
SS67221 split-GAL4 MCFO

Figure 4

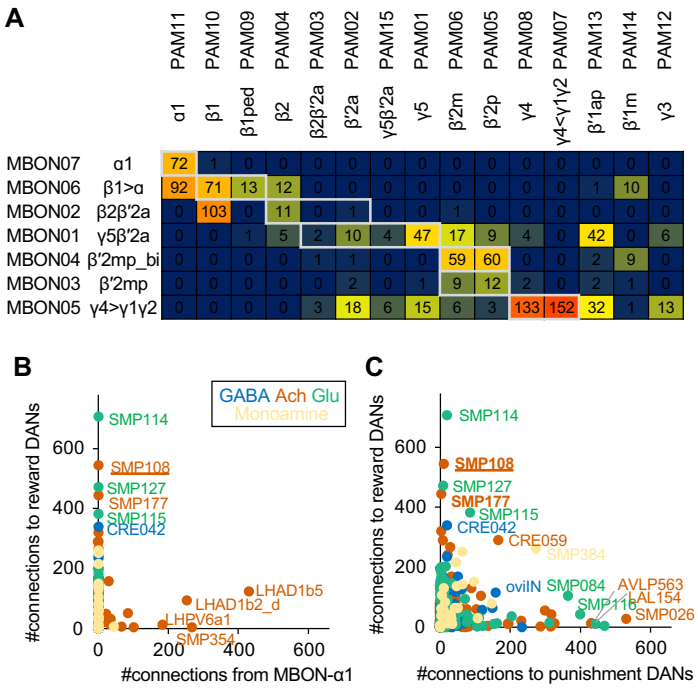

Figure 4-figure supplement 1

DAN cell type	PAM01_a	PAM01_b	PAM15_a	PAM15_b	PAM02	PAM03	PAM04_a	PAM04_b	PAM05	PAM06_a	PAM06_b	PAM07	PAM08_a	PAM08_b	PAM08_c	PAM08_d	PAM09	PAM10	PAM11	PAM12	PAM13	PAM14	PPL101	PPL102	PPL103	PPL104	PPL105	PPL106	PPL201	PPL202
MB compartments	y5	y5	y5B'2a	y5B'2a	B'2a	B2B'2a	B2	B2	B'2p	B'2m	B'2m	y4<y1y2	y4	y4	y4	y4	B1ped	B1	a1	y3	B'1ap	B'1m	y1pedc	y1	y2a1	a'3	a'2a2	a3	calyx	calyx
Total number of connectiosn from SMP108	14	19	12	4	166	4	16	9	49	153	7	5	63	1	37	10	27	17	11	1	5	3	2	5	3	2	1	4	11	5
number of cells / DAN cell type	12	7	1	2	8	4	15	1	10	11	4	5	8	5	4	1	6	6	7	11	7	8	1	1	1	1	1	1	1	1
number of connection from SMP108 / cell	1.2	2.7	12.0	2.0	20.8	1.0	1.1	9.0	4.9	13.9	1.8	1.0	7.9	0.2	9.3	10.0	4.5	2.8	1.6	0.1	0.7	0.4	2.0	5.0	3.0	2.0	1.0	4.0	11.0	5.0

Figure 4-figure supplement 2

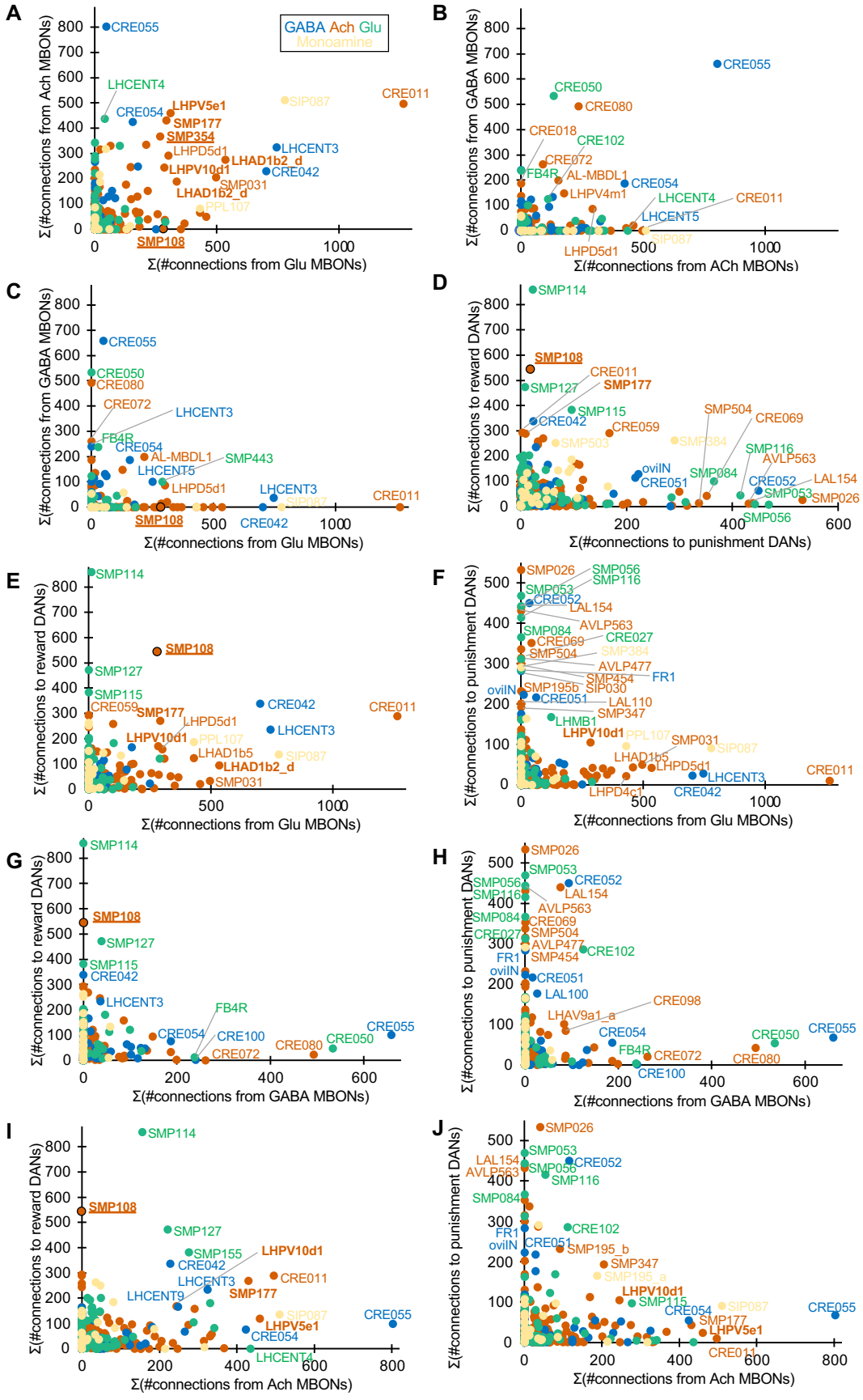

Figure 4-figure supplement 3

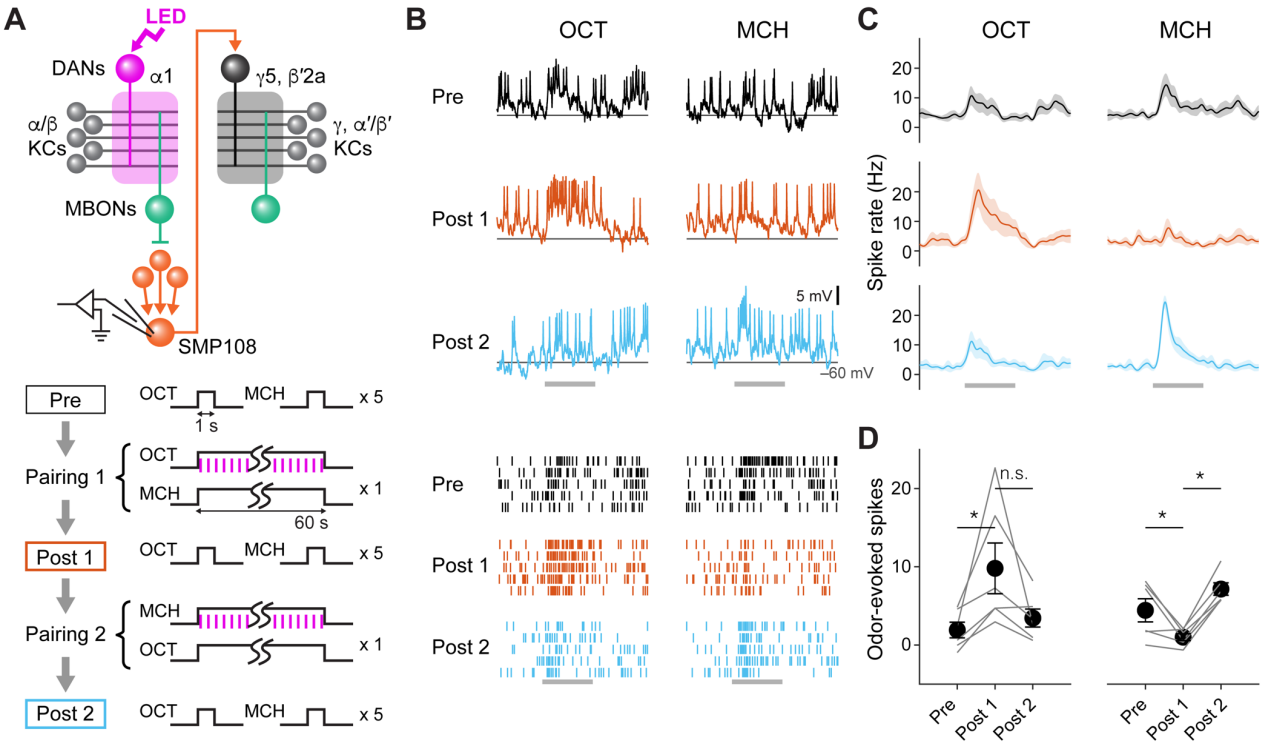
A
LED
DANs
α1
α/β
KCs
γ5, β′2a
γ, α′/β′
KCs
MBONs
SMP108
Pre
OCT
MCH
x 5
1 s
Pairing 1
OCT
MCH
x 1
60 s
Post 1
OCT
MCH
x 5
Pairing 2
MCH
OCT
x 1
Post 2
OCT
MCH
x 5
B
OCT
MCH
Pre
Post 1
Post 2
5 mV
−60 mV
C
OCT
MCH
Spike rate (Hz)
20
10
0
D
Odor-evoked spikes
n.s.
*
Pre
Post 1
Post 2

Figure 5

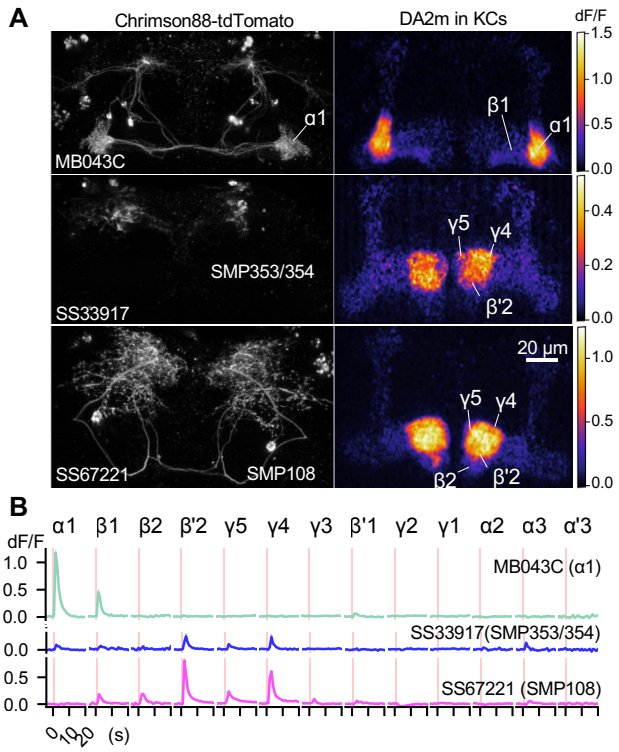
A
Chrimson88-tdTomato
DA2m in KCs
dF/F
1.5
1.0
0.5
0.0
α1
β1
α1
MB043C
0.4
0.2
0.0
γ5
γ4
SMP353/354
SS33917
β'2
20 μm
1.0
0.5
0.0
γ5
γ4
SS67221
SMP108
β2
β'2
B
α1 β1 β2 β'2 γ5 γ4 γ3 β'1 γ2 γ1 α2 α3 α'3
dF/F
1.0
0.5
0.0
MB043C (α1)
0.0
SS33917(SMP353/354)
0.5
0.0
SS67221 (SMP108)
0 10 20 (s)

Figure 6

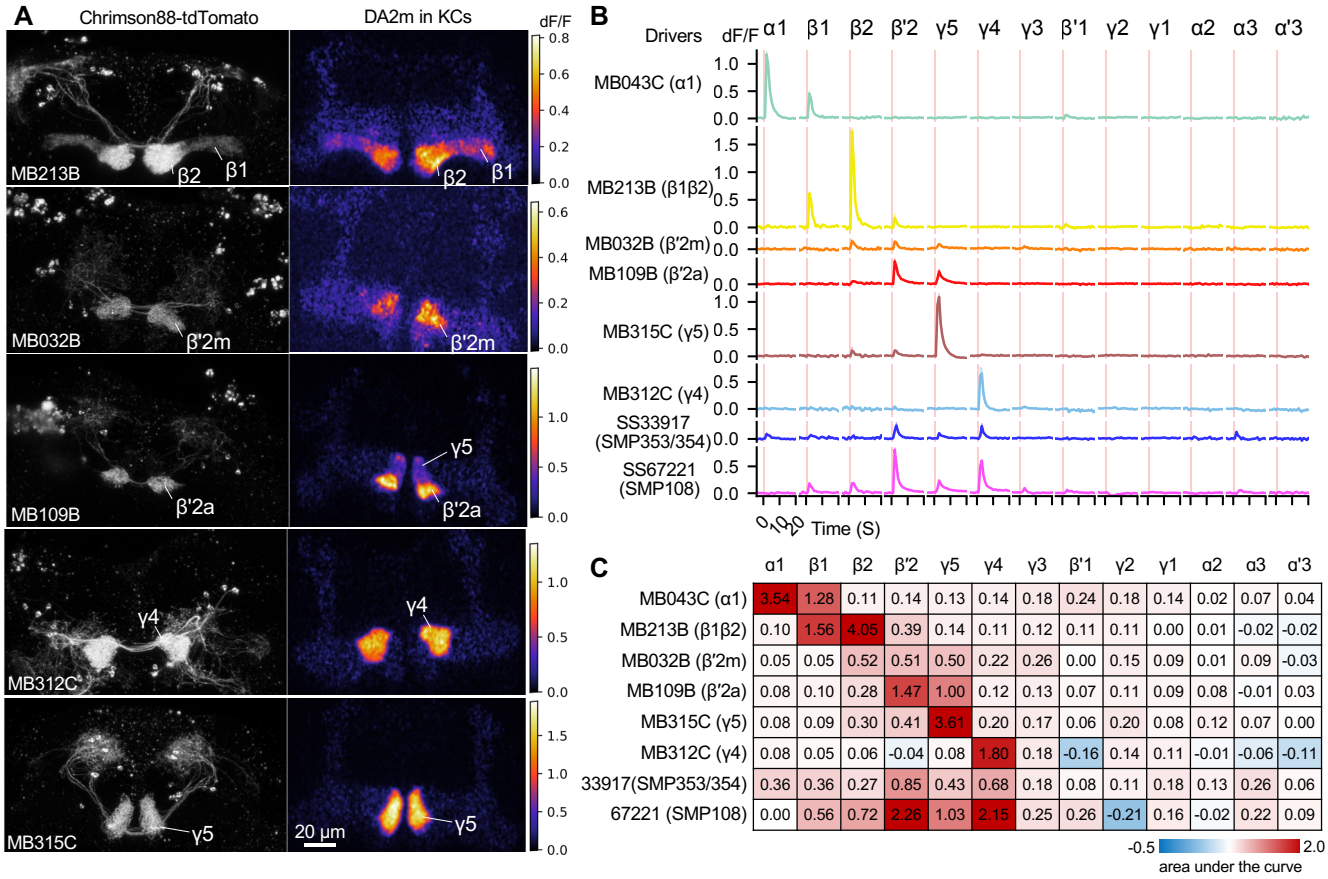

Figure 6-figure supplement 1

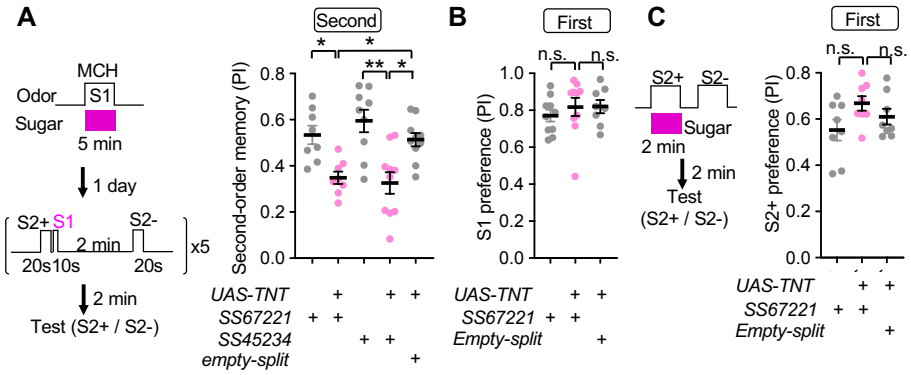
A
MCH
Odor
S1
Sugar
5 min
1 day
S2+ S1
S2-
2 min
20s 10s
20s
x5
2 min
Test (S2+ / S2-)
Second
Second-order memory (PI)
0.8
0.6
0.4
0.2
0.0
*
*
**
*
UAS-TNT + + + +
SS67221 + +
SS45234 + +
empty-split +
B
First
S1 preference (PI)
1.0
0.8
0.6
0.4
0.2
0.0
n.s.
n.s.
UAS-TNT + +
SS67221 + +
Empty-split +
C
S2+ S2-
Sugar
2 min
2 min
Test
(S2+ / S2-)
First
S2+ preference (PI)
0.8
0.6
0.4
0.2
0.0
n.s.
n.s.
UAS-TNT + +
SS67221 + +
Empty-split +

Figure 7

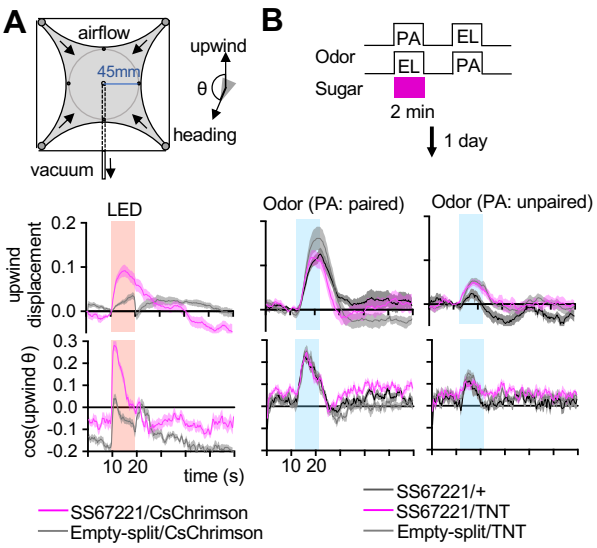

Figure 7-figure supplement 1

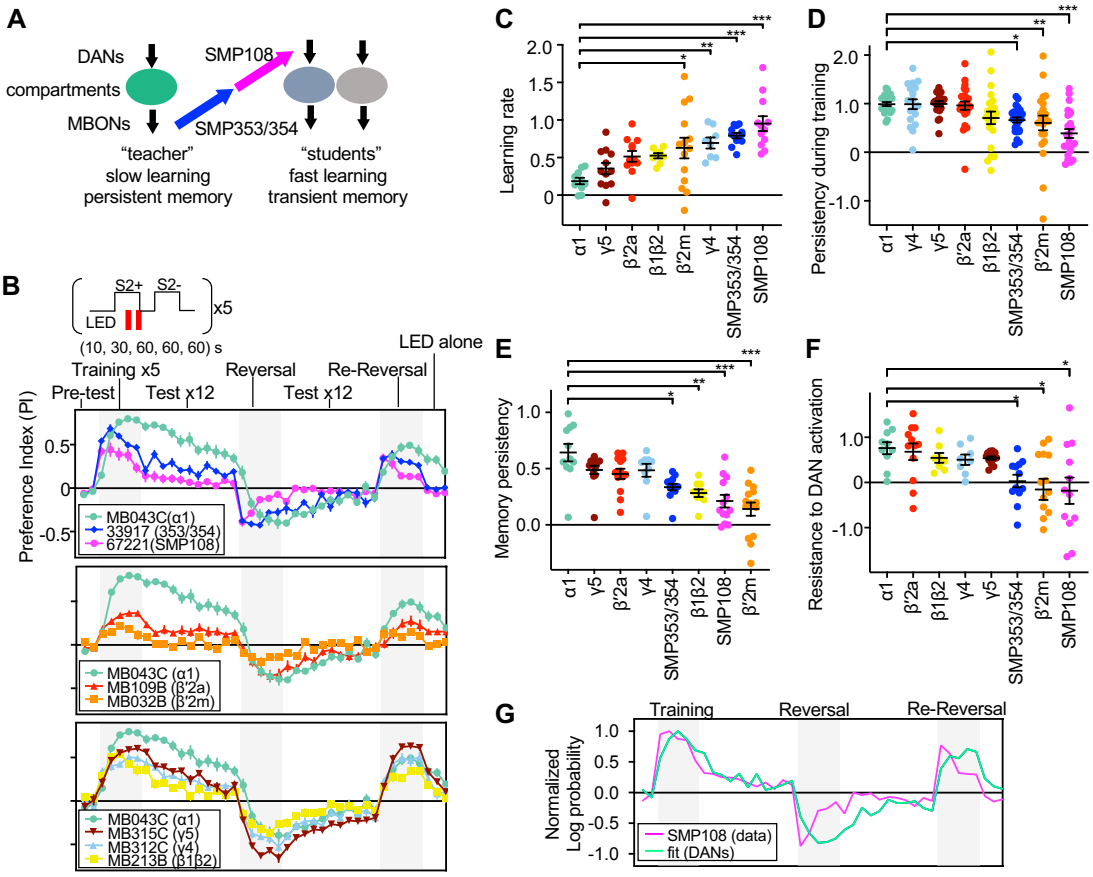
A
DANs
compartments
MBONs
SMP108
SMP353/354
"teacher"
slow learning
persistent memory
"students"
fast learning
transient memory
B
S2+
S2-
LED
x5
(10, 30, 60, 60, 60) s
LED alone
Training x5
Reversal
Re-Reversal
Pre-test
Test x12
Test x12
Preference Index (PI)
MB043C(α1)
33917 (353/354)
67221(SMP108)
MB043C (α1)
MB109B (β'2a)
MB032B (β'2m)
MB043C (α1)
MB315C (γ5)
MB312C (γ4)
MB213B (β1β2)
C
Learning rate
α1
γ5
β'2a
β1β2
β'2m
γ4
SMP353/354
SMP108
D
Persistency during training
E
Memory persistency
F
Resistance to DAN activation
G
Training
Reversal
Re-Reversal
Normalized
Log probability
SMP108 (data)
fit (DANs)

Figure 8

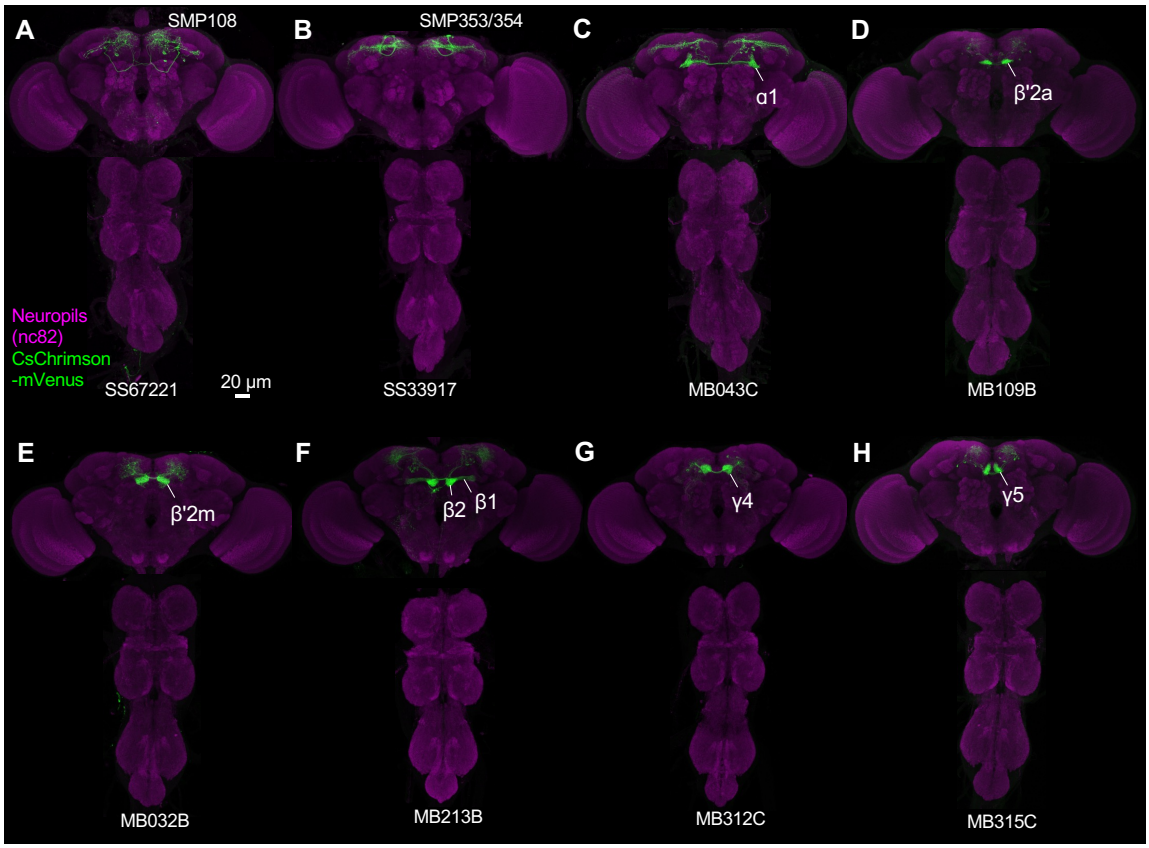

Figure 8-figure supplement 1 Expression patterns of drivers